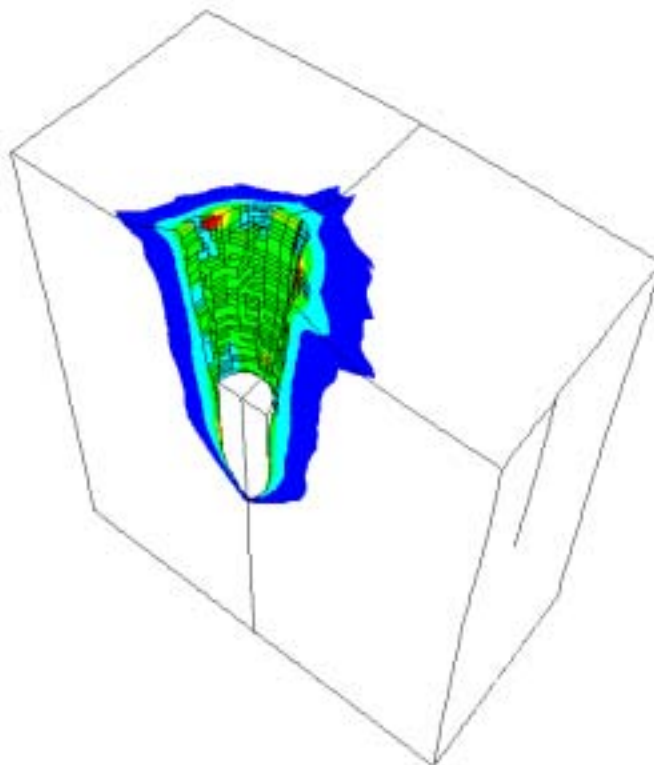


Mattias Unosson

## **Numerical simulations of penetration and perforation of high performance concrete with 75mm steel projectile**



DEFENCE RESEARCH ESTABLISHMENT

Weapons and Protection Division

SE-147 25 TUMBA

FOA-R--00-01634-311--SE

November 2000

ISSN 1104-9154

Mattias Unosson

# **Numerical simulations of penetration and perforation of high performance concrete with 75mm steel projectile**

Distribution: HKV/KRI/PLAN/Anläggning, FortV, FHS, FFI, Dynalis, Engineering Research AB, EMI  
Freiburg, Karagozian & Case

FOA: FOA Program, FOA 2

<b>Issuing organization</b> Defence Research Establishment Weapons and Protection Division SE-147 25 TUMBA SWEDEN	<b>Document ref. No., ISRN</b> FOA-R--00-01634-311--SE	
	<b>Date of issue</b> November 2000	<b>Project No.</b> E2614
	<b>Project name (abbrev. if necessary)</b> HPC	
<b>Author(s)</b> Mattias Unosson	<b>Initiator or sponsoring organization</b> Swedish Defence Headquarter	
	<b>Project manager</b> Anders Carlberg	
	<b>Scientifically and technically responsible</b>	
<b>Document title</b> Numerical simulations of penetration and perforation of high performance concrete with 75mm steel projec		
<b>Abstract</b> <p>In the report, simulations of penetration and perforation of three types of high performance concrete (HPC) targets are presented and compared with experimental data. The objective of the simulations was to assess the chosen concrete material model's ability to predict depth of penetration or residual velocity. The tests were simulated numerically with the code LS-DYNA and the standard material type 72, "Concrete Damage". Lagrangian solution technique was used together with numerical erosion based on a shear strain criteria. For the perforation good agreement with test data was achieved but in the case of penetration, the results were not satisfying.</p>		
<b>Keywords</b> Numerical simulation, LS-DYNA, high performance concrete, penetration, perforation, steel projectile		
<b>Further bibliographic information</b>		<b>Language</b> English
<b>ISSN</b> 1104-9154		<b>ISBN</b>
		<b>Pages</b> 67 p.
<b>Distributor (if not issuing organization)</b>		

<b>Dokumentets utgivare</b> Försvarets forskningsanstalt Avdelningen för Vapen och skydd SE-147 25 TUMBA	<b>Dokumentbeteckning, ISRN</b> FOA-R--00-01634-311--SE	
	<b>Dokumentets datum</b> november 2000	<b>Uppdragsnummer</b> E2614
	<b>Projektamn (ev förkortat)</b> HPC	
<b>Upphovsman(män)</b> Mattias Unosson	<b>Uppdragsgivare</b> HKV	
	<b>Projektansvarig</b> Anders Carlberg	
	<b>Fackansvarig</b>	
<b>Dokumentets titel</b> Numeriska simuleringar av penetration och perforation av högpresterande betong med 75mm stålprojektil		
<b>Sammanfattning</b> <p>I rapporten presenteras simuleringar av perforation och penetration i tre typer av mål gjutna av höpresterande betong och resultaten jämföres med försöksdata. Syftet med simuleringarna var att utvärdera den valda materialmodellens förmåga att förutsäga penetrationsdjup eller projektilens residualhastighet. Försöken simuleras med koden LS-DYNA och materialtyp 72, "Concrete damage". Lagrangeteknik tillämpas på problemet tillsammans med numerisk erosion baserad på skjuttöjning. För perforation är överensstämmelsen med försöksdata god men för penetration är överensstämmelsen ej tillfredsställande.</p>		
<b>Nyckelord</b> Numerisk simulering, LS-DYNA, högpresterande betong, penetration, perforation, stålprojektil		
<b>Övriga bibliografiska uppgifter</b>	<b>Språk</b> Engelska	
<b>ISSN</b> 1104-9154	<b>ISBN</b>	
	<b>Omfång</b> 67 s.	

**Distributör (om annan än ovan)**

**CONTENTS**

- 1 INTRODUCTION ..... 5**
- 2 TESTS ..... 6**
- 3 MATERIAL CHARACTERISATION .....12**
  - 3.1 Target..... 12
  - 3.2 Projectile ..... 12
- 4 NUMERICAL SIMULATIONS.....14**
  - 4.1 Target 1-3 ..... 21
  - 4.2 Target 4-6..... 28
  - 4.3 Target 7-9..... 34
- 5 SUMMARY..... 39**
- REFERENCES..... 40**
- APPENDICES .....41**
  - Appendix A ..... 41
  - Appendix B ..... 45
  - Appendix C ..... 52
  - Appendix D ..... 54
  - Appendix E ..... 57
  - Appendix F ..... 60
  - Appendix G..... 63

## 1 INTRODUCTION

The simulations in this report were part of the HPC-project in which the following Swedish and Norwegian organisations co-operated during the years 1997 – 2000 to build up their competence in high strength concrete (HPC):

Sweden

- Armed Forces Headquarter (HKV), <http://www.mil.se/>
- Defence Research Establishment (FOA), <http://www.foa.se/>
- Fortification Administration (FortV), <http://www.fortv.se/>

Norway

- Headquarters Defence Command (FO), <http://www.fo.mil.no/>
- Defence Research Establishment (FFI), <http://www.ffi.no/>
- Defence Construction Service (FBT), <http://www.mil.no/fbt>

The penetration and perforation test, upon which the simulations presented in this report are based on, were performed in Karlskoga at the Bofors Testing Centre (<http://www.bofors.se/testcenter>) 1999-10-05—07 comprising nine tests at three types of cylindrical concrete targets.

## 2 TESTS

A 6.3kg armour piercing steel projectile with an ogival nose radius of 127mm, a length of 225mm and diameter of 75mm was fired at the targets, see Figure 1. The projectile impacted with approximately zero angle of attack and a velocity of about 620m/s (cf. Figure 2 and Figure 3). Targets 1-3 were penetration tests (projectile comes to rest in the target) and targets 4-9 were perforation tests (projectile passes through target). In Table 1 the target specifications and global test results are presented.

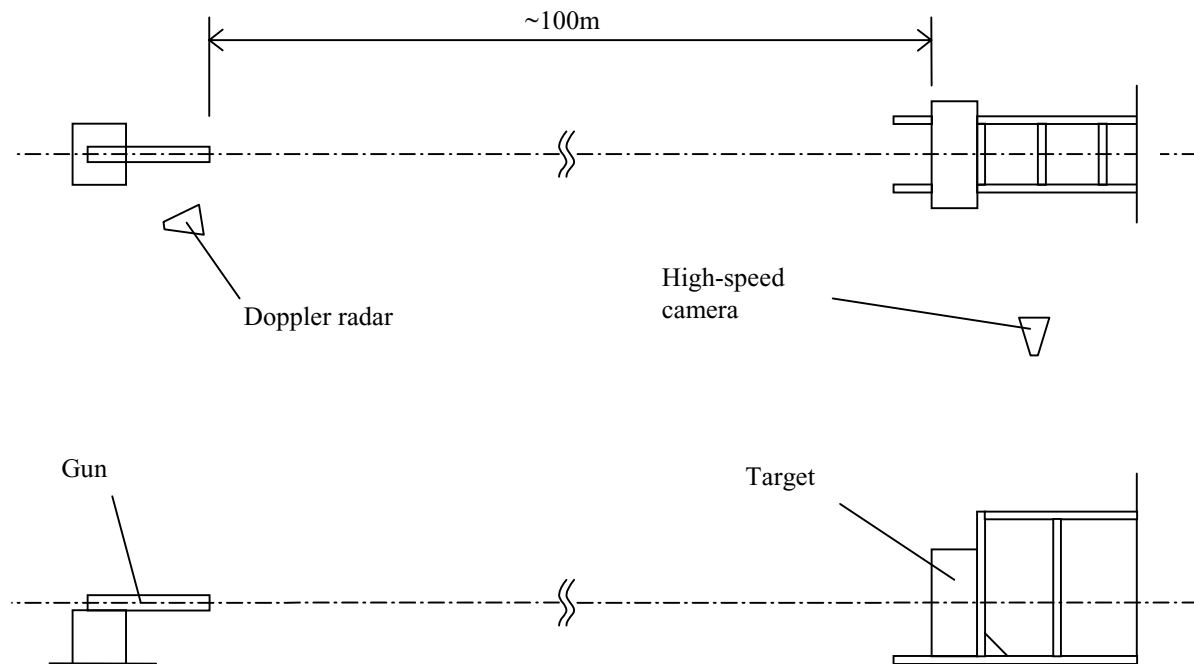


**Figure 1. Experimental set up**

**Table 1. Target specifications and test results**

Target number	Diameter [mm]	Length [mm]	Reinforcement mass ratio	Projectile impact velocity [m/s]	Depth of penetration [mm]	Projectile residual velocity [m/s]
1	1 400	800	0.00	617	450	-
2	1 400	800	0.00	612	540	-
3	1 400	800	0.00	619	510	-
4	1 400	400	0.00	616	-	276*
5	1 400	400	0.00	616	-	303*
6	1 400	400	0.00	618	-	293*
7	1 400	400	0.06	617	-	Not measured
8	1 400	400	0.06	616	-	Not measured
9	1 400	400	0.06	616	-	260

\*: Data from FFI



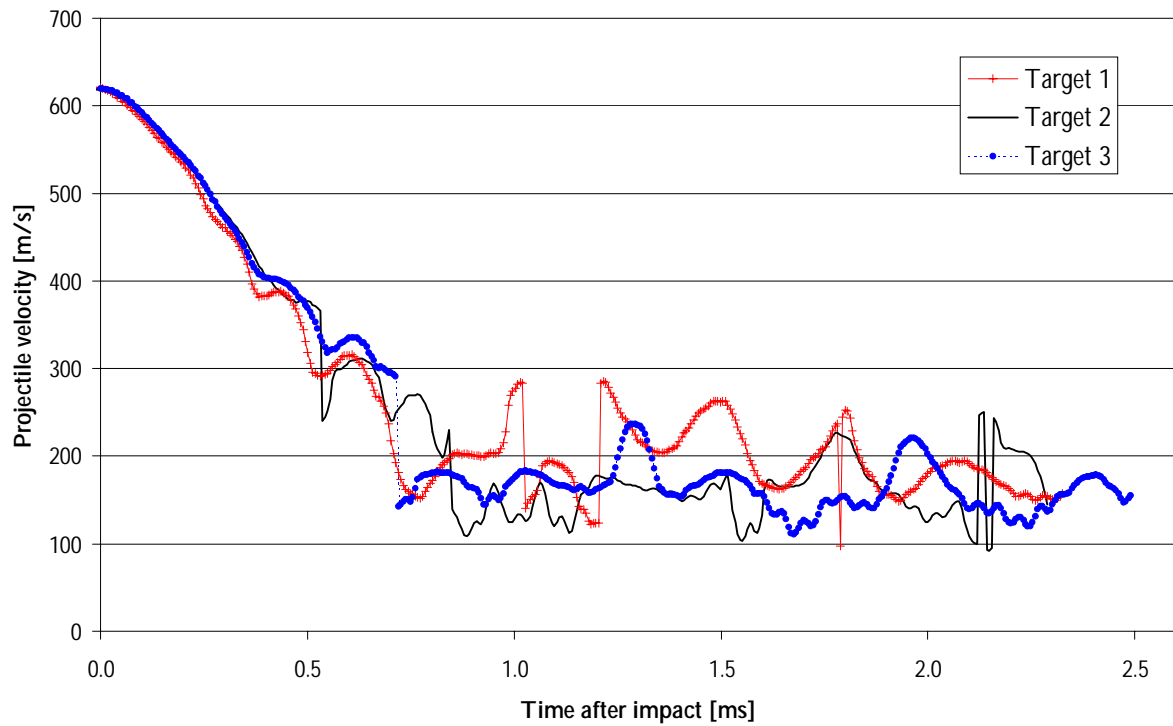


Figure 6. Projectile velocity versus time for targets 1-3.

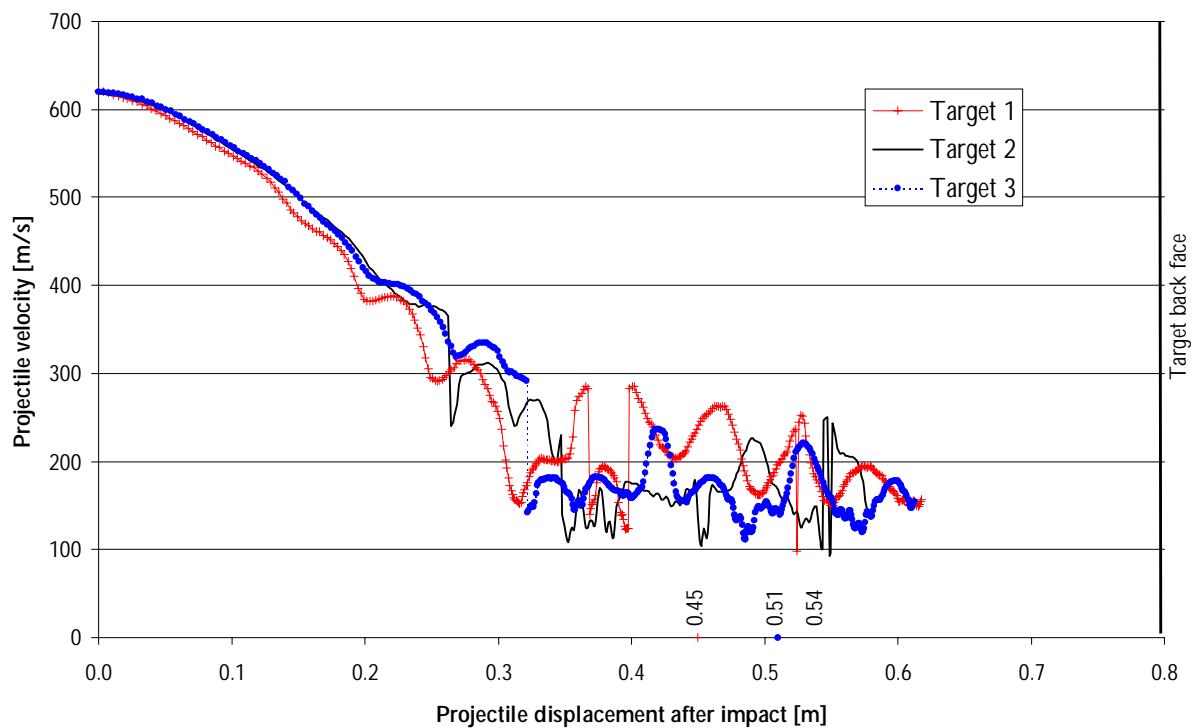
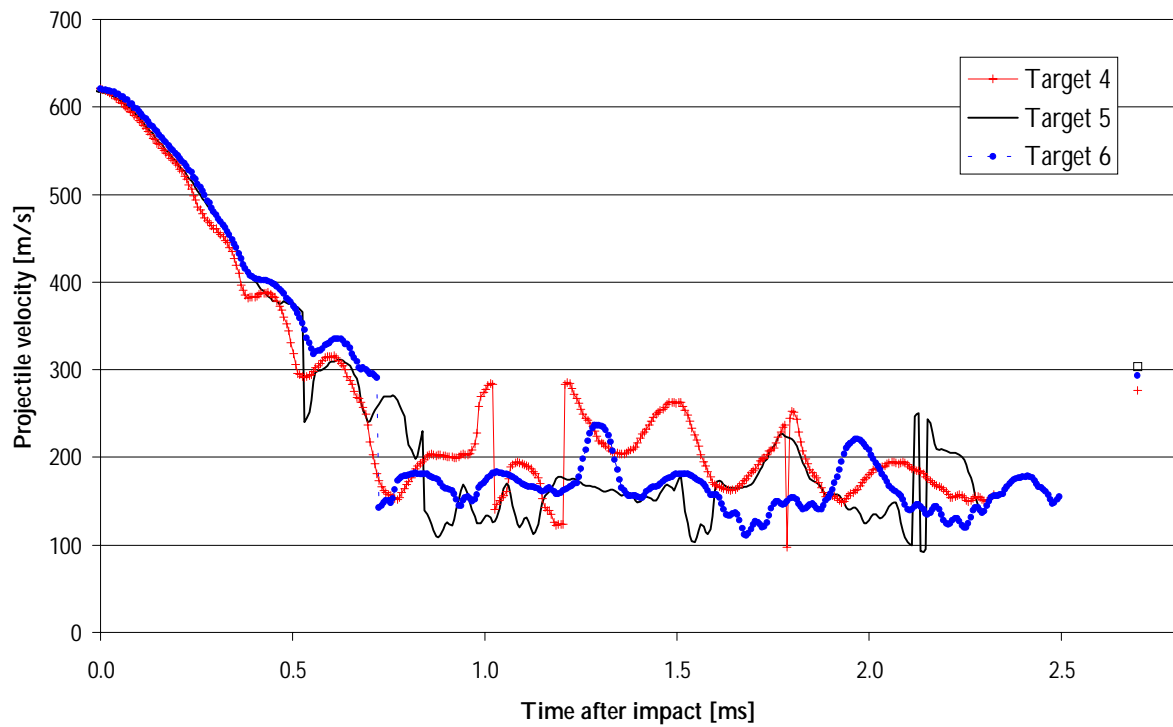
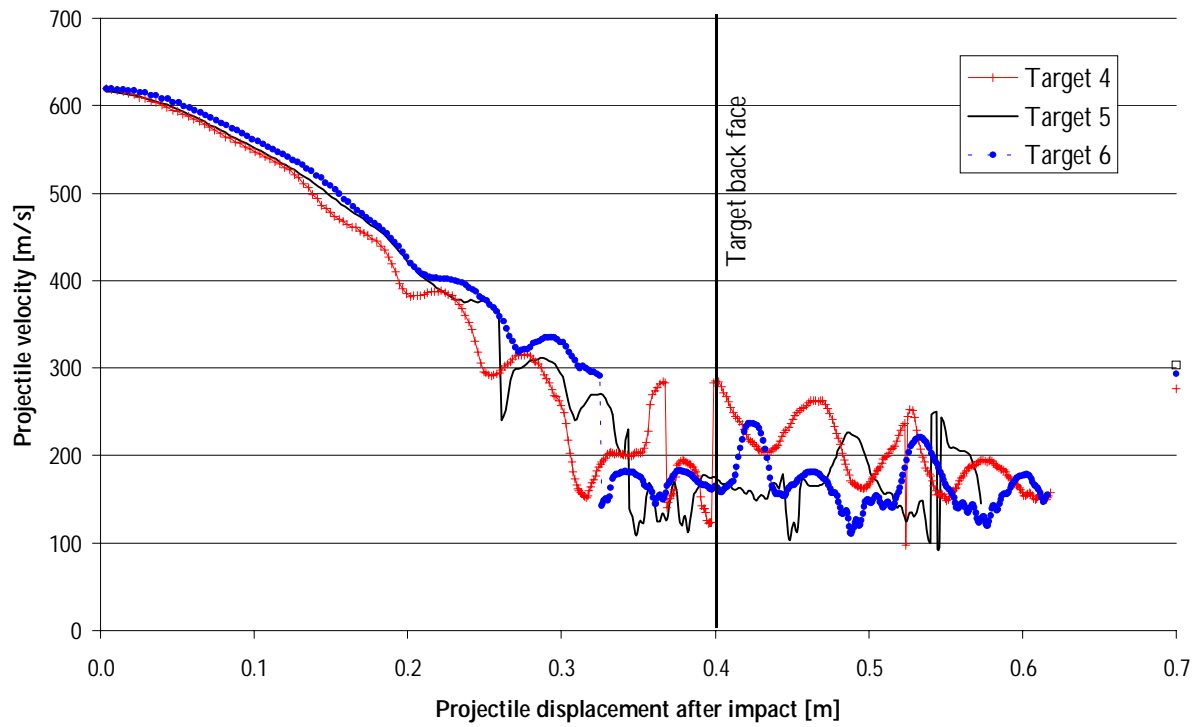


Figure 7. Projectile velocity versus displacement for targets 1-3 (including three points for the post-test measured depth of penetration).



**Figure 8.** Projectile velocity versus time for targets 4-6 (including three data points from the high-speed camera).



**Figure 9.** Projectile velocity versus displacement for targets 4-6 (including three data points from the high-speed camera).

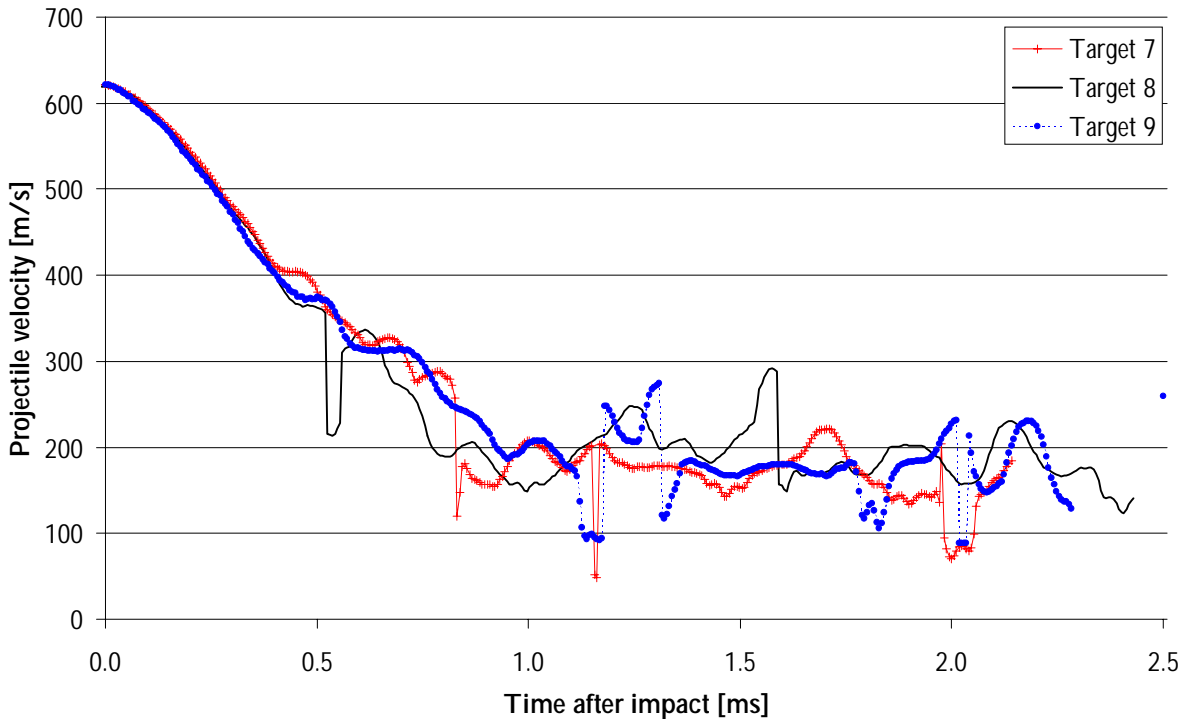


Figure 10. Projectile velocity versus time for targets 7-9 (including one data point from the high-speed camera).

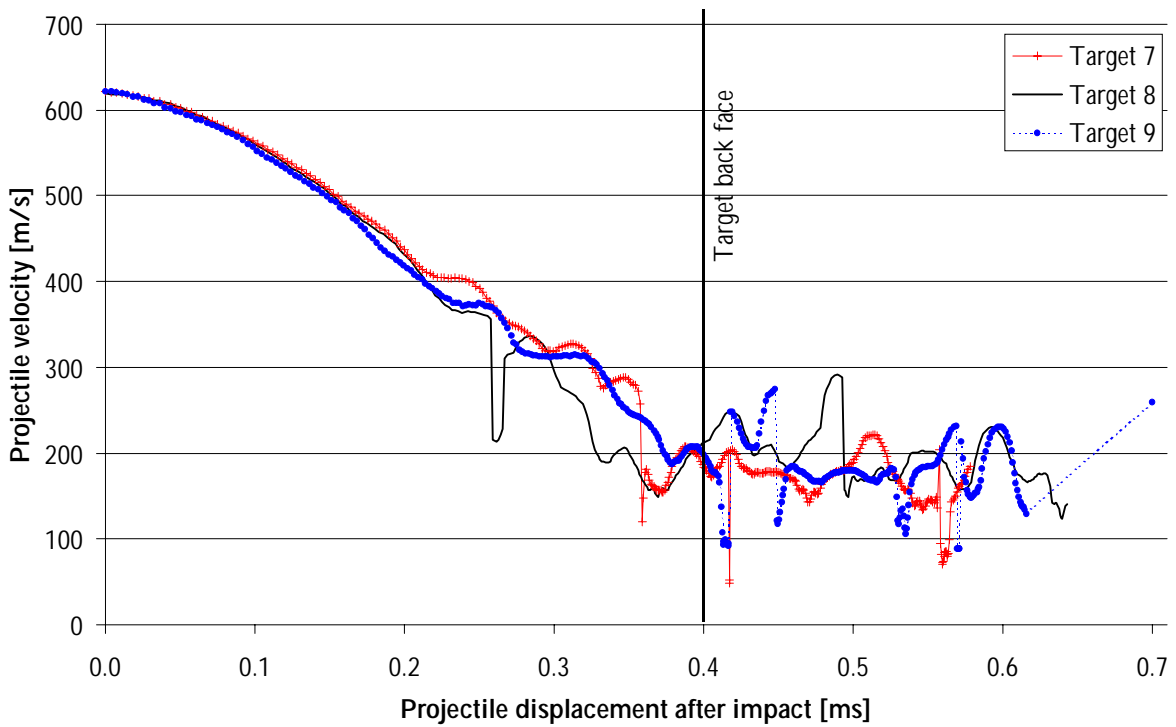


Figure 11. Projectile velocity versus displacement for targets 7-9 (including one data points from the high-speed camera).

When using only one Doppler radar it is not possible to distinguish signals from objects moving towards the radar from objects moving away from the radar. Therefore the data in the above figures should only be used as guidance.

### 3 MATERIAL CHARACTERISATION

#### 3.1 Target

Standard material testing was performed on 150x150mm cubes for the unconfined uniaxial compressive strength, 100x200mm cylinders for the splitting tensile strength and the modulus of elasticity. Determination of the fracture energy was done according to RILEM "Determination of the fracture energy of mortar and concrete". The results are presented in Table 2.

**Table 2. Concrete material test data**

Mass density	Uniaxial compressive strength	Splitting tensile strength	Modulus of elasticity	Fracture energy
2 770kg/m <sup>3</sup>	153MPa	9.1MPa	58GPa	162N/m

By default the Poisson's constant is taken as 0.16 and the uniaxial tensile strength is taken as 90% of the split strength according to The Swedish Concrete Handbook [4].

For the reinforcement the parameters in Table 3 were taken from earlier tests performed on the same type of reinforcement, 12mm rebars with quality KS500ST. The strain at maximum force (peak strain) was determined according to ISO 10606:1995(E).

**Table 3. Reinforcement material test data.**

Mass density	Yield stress	Poisson's ratio	Modulus of elasticity	Hardening modulus	Peak strain
7 800kgm <sup>-3</sup>	586MPa	0.3	207GPa	1.1GPa	0.092

#### 3.2 Projectile

The Vicker's test (HV10) was performed on one of the projectiles after the tests and the yield limit was calculated according to the following relationship.

$$f_{sy} \approx \frac{100 \cdot 10^6}{32} HV_{10}$$

The results from the Vicker's test together with the calculated yield limit is presented in Figure 12 and the parameters in Table 4 were chosen from standard steel data.

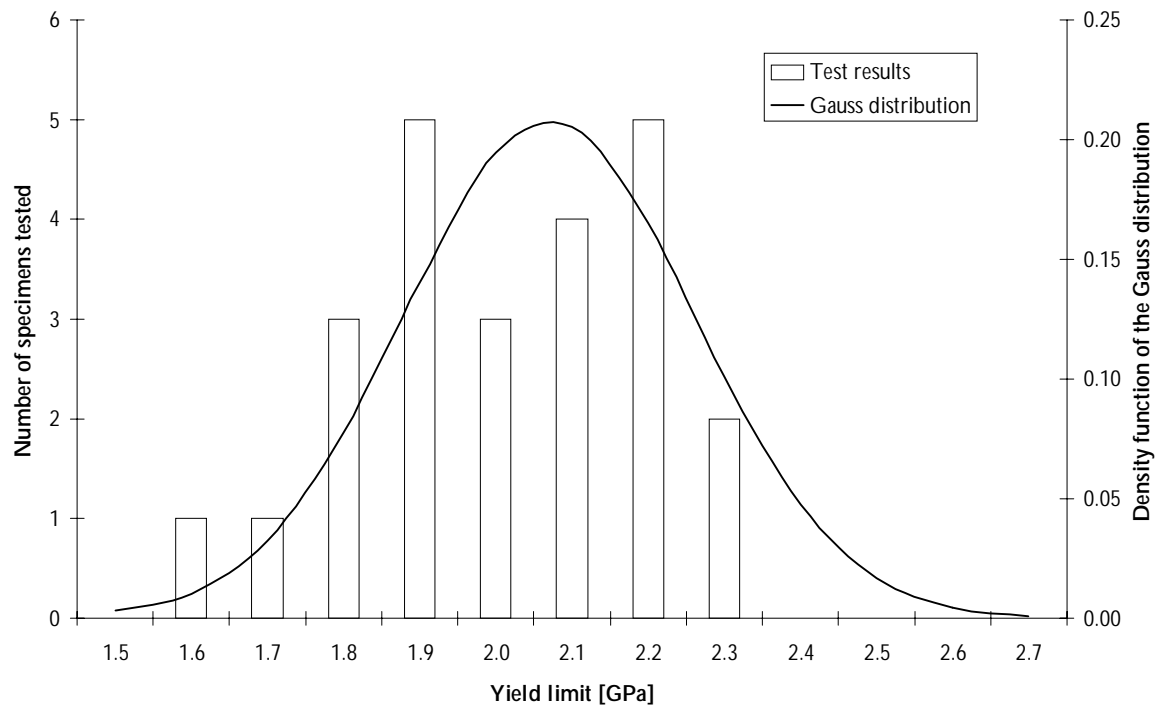


**Figure 12. Results from the Vicker's test (HV10) performed on a projectile after tests.**

**Table 4. Projectile elastic material parameters.**

Mass density	Modulus of elasticity	Poisson's ratio
7 800kg/m <sup>3</sup>	200GPa	0.3

## 4 NUMERICAL SIMULATIONS

The tools used for the simulations are specified in Table 5.

The geometry was modelled with two symmetry planes and both the target and the projectile were described in material or Lagrangian co-ordinates. All nodes on the target's perimeter were constrained to no displacement in the direction of the projectiles path. For the contact between target and projectile, the standard LS-DYNA algorithm "eroding surface to surface" was used. This is the only available contact algorithm that can be used together with numerical erosion, i.e. that updates the contact surfaces after each computational time step to account for eroded elements.

The target was modelled using 8-node solid elements and an erosion criterion based on shear strain. The numerical erosion can only be used with solid elements and 1-point integration. The critical erosion value had to be determined through an iterative procedure, which is presented in chapter 4.2. For the target elements, hourglass control of the type Flanagan-Belytschko stiffness form with exact volume integration were used. For the target the LS-DYNA material type 72 "Concrete Damage" was used, see Appendix B for a detailed presentation of the material model. Since neither the material type number 72 or the numerical erosion option is available in the pre-processor LS-INGRID changes had to be done in the LS-DYNA input file.

The projectile was modelled using 8-node solid elements with 8-points integration and an elastic material model, LS-DYNA material type 2. The same mesh was used for all simulations and specifications are given in Table 6.

The reinforcement was modelled using 2-node truss elements and the LS-DYNA elastic material type 2 together with the material parameters given in Table 3.

**Table 5. System specifications.**

Compaq Workstation XP1000
667 MHz DEC/Alpha 21264A processor with 1024 MB main memory
Digital UNIX version 4.0d
LS-INGRID versions 3.5a and 3.5b [6]
LS-DYNA version 950c [1]
LS-TAURUS version 940.3 [3]

**Table 6. Mesh data for projectile**

Nodes	484
Solid elements	252
Characteristic element size	7.5 mm

Now follows a detailed explanation of the chosen input data for the target. The maximum compression meridian was fitted to the one given by the CEB-FIP Model Code 1990 [5] and the initial compression yield meridian and the residual compression meridian were constructed according to the instructions in [2]. In Figure 13 three different stress-paths are drawn together with the maximum compression meridian. In Figure 14 both the compression and tension meridians are shown for pressure up to 1.7GPa.

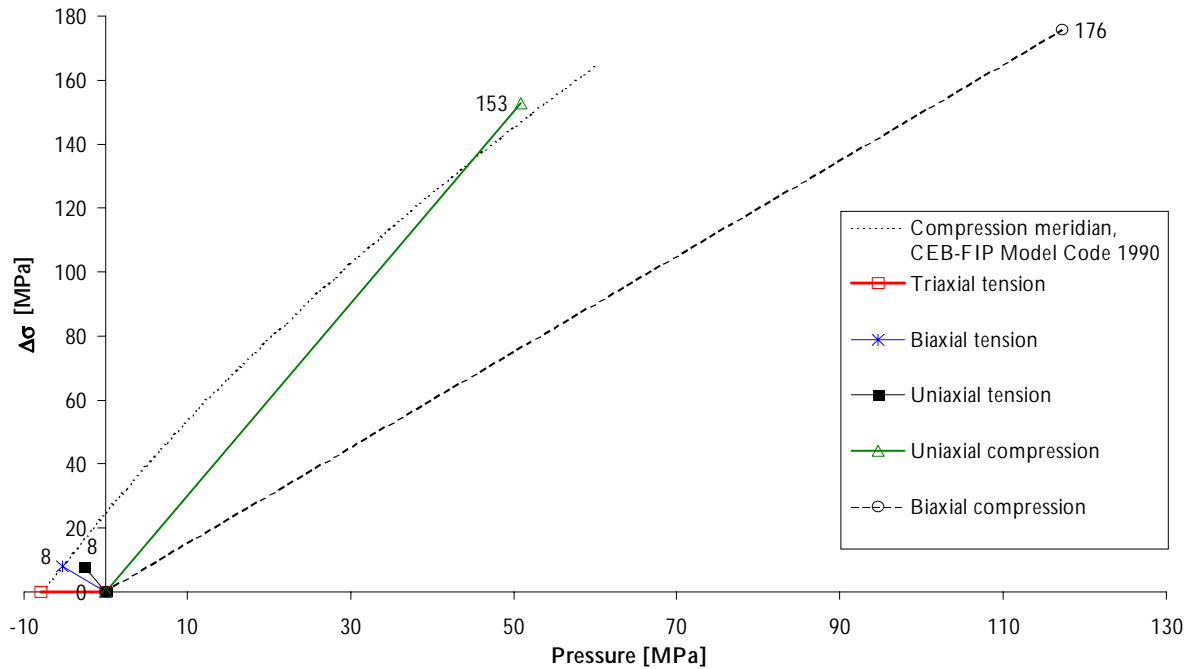


Figure 13. Compressive meridian and test stress paths.

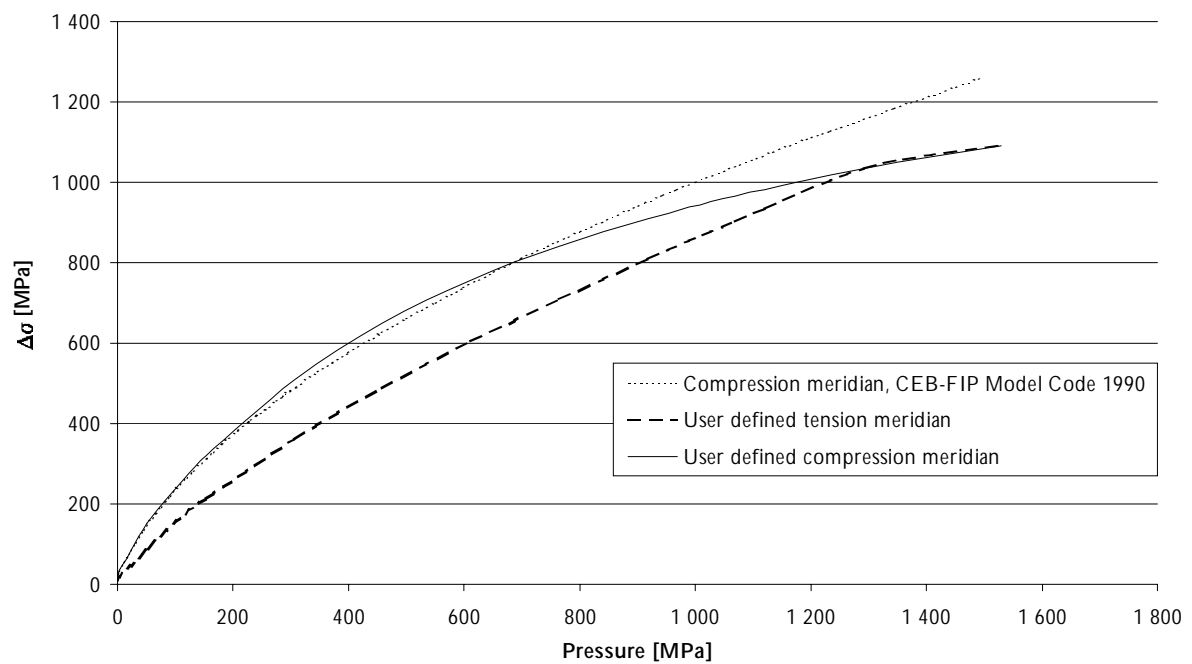
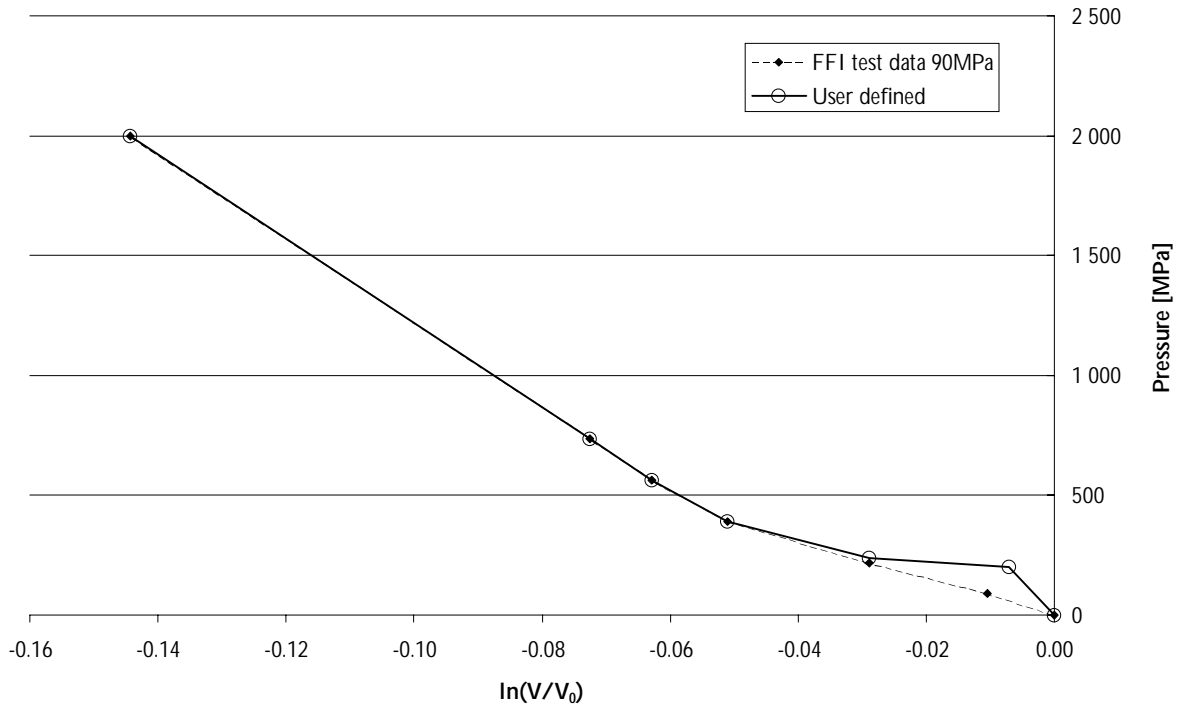


Figure 14. Compressive and tensile meridian used for the simulations.



**Figure 15. Equation of state used for the simulations.**

For the equation of state, a combination of test data from FFI on concrete with cube strength of 90MPa and the data given in table 1 on the modulus of elasticity was used. The slope of the elastic-porous part was calculated as:

$$K = \frac{E}{3(1-2\nu)} = \frac{58}{3(1-2 \cdot 0.16)} = 28.43 \text{ GPa}$$

The curve was then connected to the FFI-curve. The difference in inclination for the elastic part is due to the GREAC-cell method used for the FFI-tests. It has been shown that this testing method gives a weaker response than that of a stabilised HOEK-cell [7]. The last point on the curve was extrapolated and the resulting equation of state is shown in Figure 15.

In the model, there are three parameters which controls the shape of the response curves, b1 for uniaxial compression, b2 for uniaxial tension and b3 for tri-axial tension. The value for b1 was taken according to the recommendations in [1]. To regularise the fracture energy release these parameters has to be determined for each element size to be used so that

$$G_f = h \int_{\varepsilon} \sigma(\varepsilon) d\varepsilon = 162 \text{ Nm}^{-1}$$

where

$$h = \sqrt[3]{V_0^{element}}$$

The damage parameters were determined by simulations of a direct tension test. The softening part of the response was fitted to the following analytical expression using a bilinear softening curve.

$$\sigma_{ct}(w) = f_{ct} e^{\left(\frac{-f_{ct} w}{G_f}\right)}$$

The resulting damage curve is shown in Figure 16.

For the two element sizes that were to be used in the simulations, 5 and 7.5mm, the damage parameters were tuned to get the right fracture energy. The resulting response curves for uniaxial compression, uniaxial tension and triaxial tension are shown in Figure 17 to Figure 19. The LS-Ingrid input file, valid for uniaxial and triaxial tension test and uniaxial compression test depending on which command lines that are commented out, is found in Appendix B. According to [2] this tuning of damage parameters is enough to avoid mesh dependency.

To assure that the input curve for strain rate dependency covered the whole range of strain rates occurring in the simulations, registrations of the effective strain rates (upon which the strength enhancement in the model is based) were made for three elements in the impact area, see (Figure 20). At time 0.022ms the first element, element 1 is eroded.

The suggested bilinear relationship for the dynamic increase factor (DIF) in [5] is valid for strain rates up to 300/s. In Figure 21 this relationship is plotted up to the observed strain-rate values.

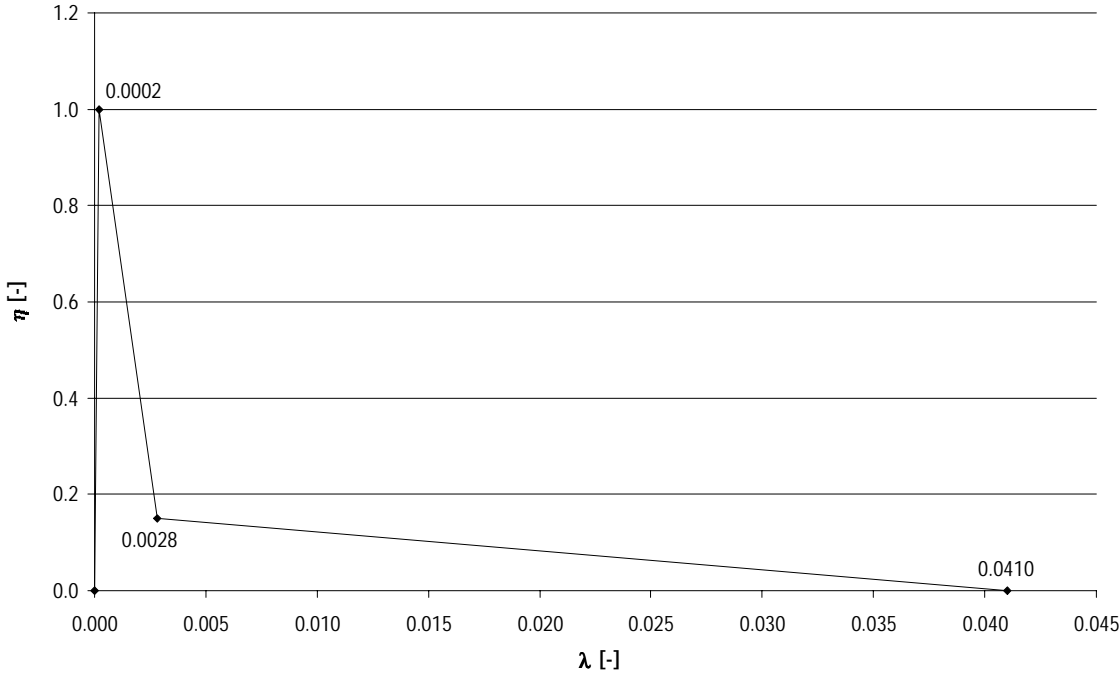


Figure 16. Damage curve used in the simulations.

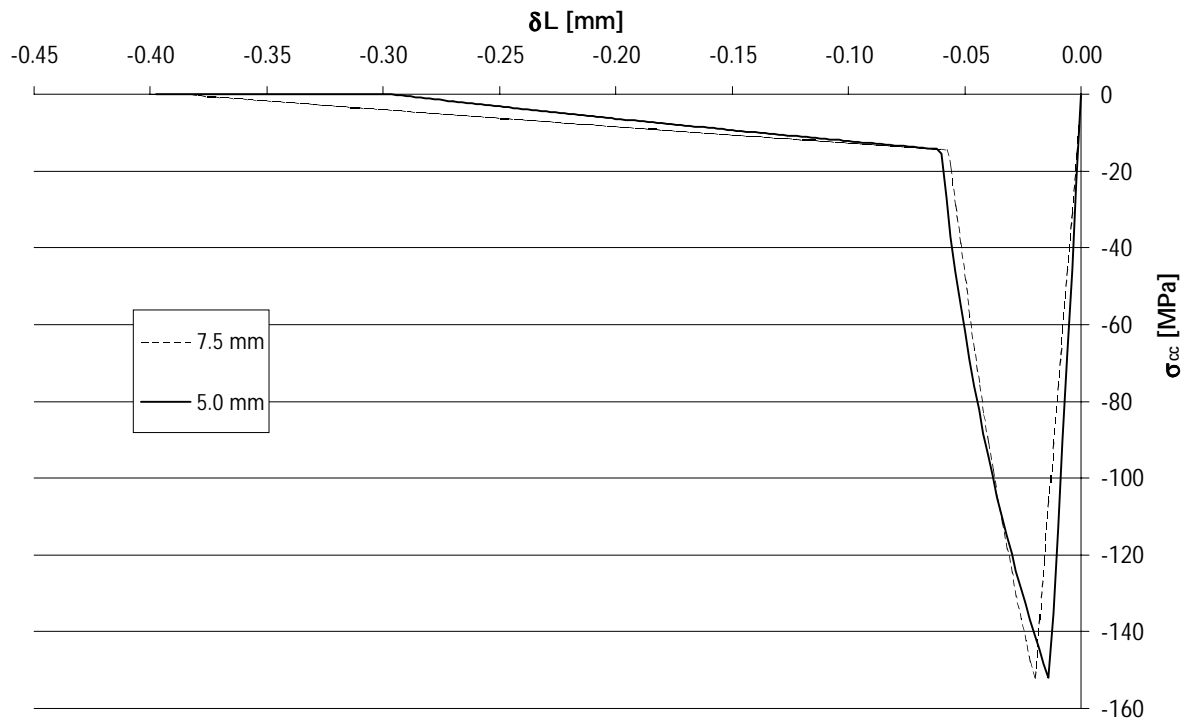


Figure 17. Response curves for element sizes 5 and 7.5 mm in uniaxial compression.

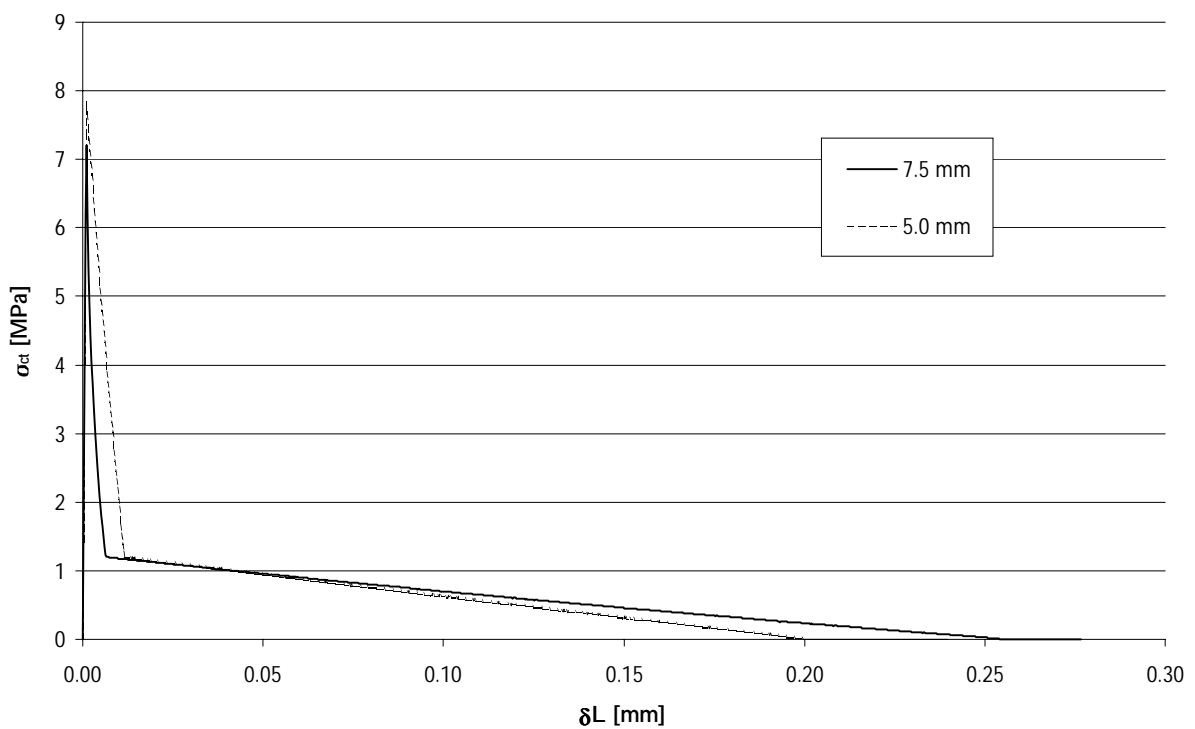


Figure 18. Response curves for element sizes 5 and 7.5 mm in uniaxial tension.

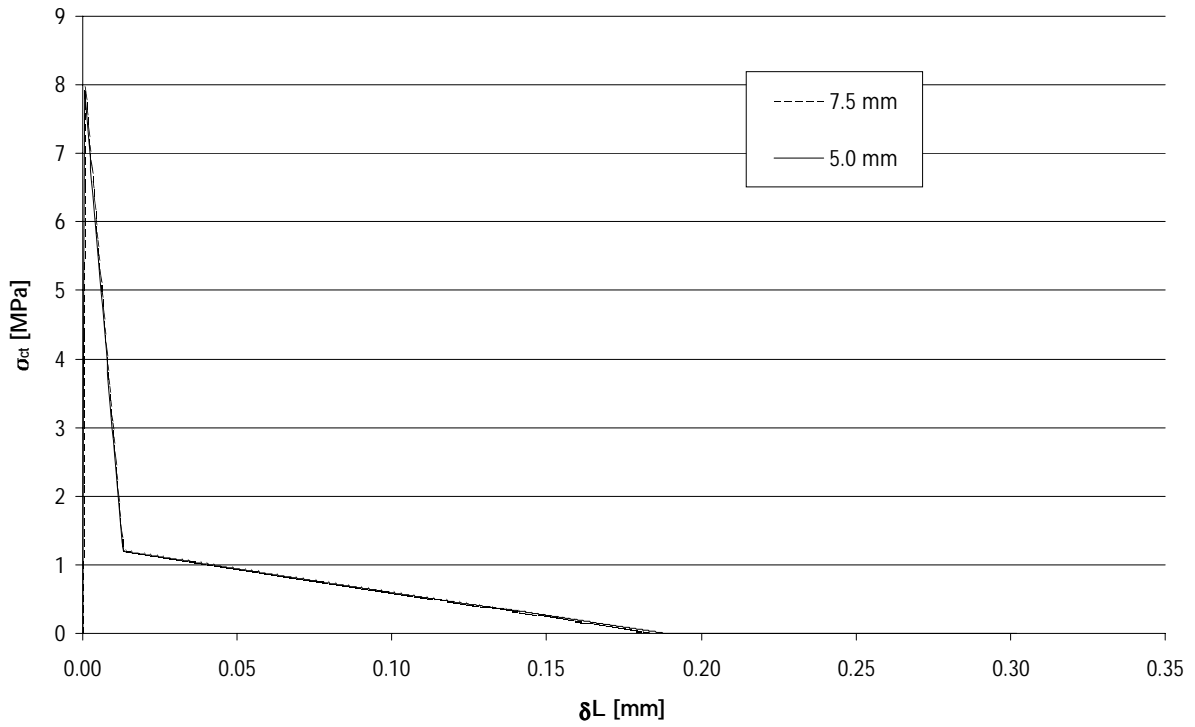


Figure 19. Response curves for element sizes 5 and 7.5 mm in triaxial tension.

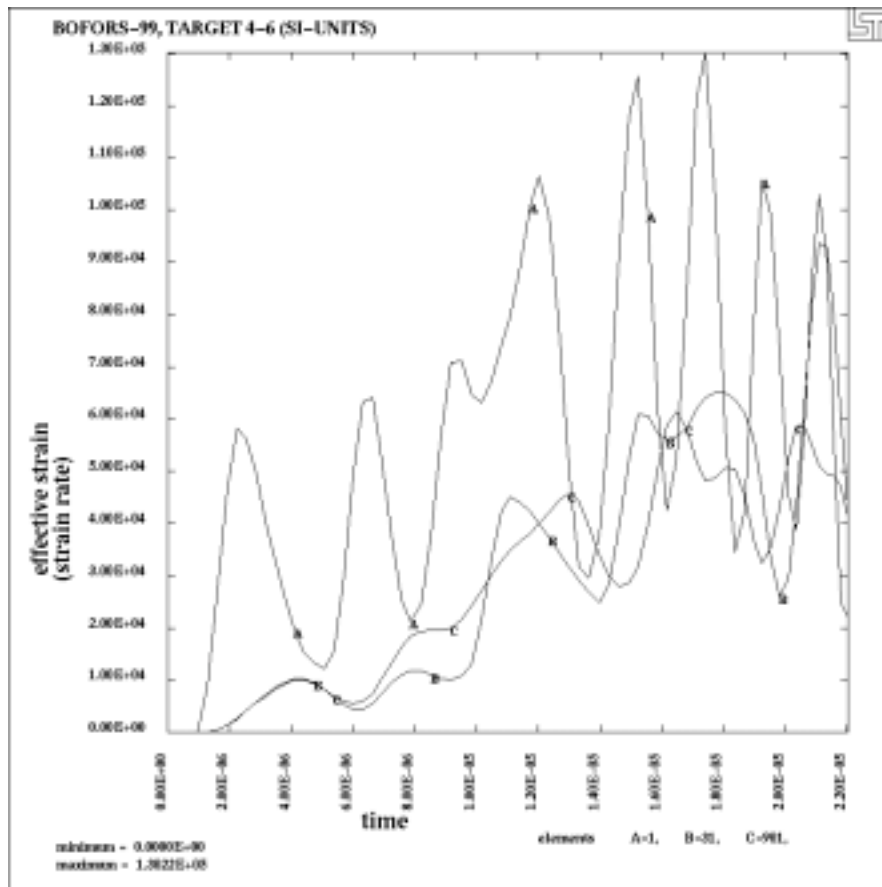
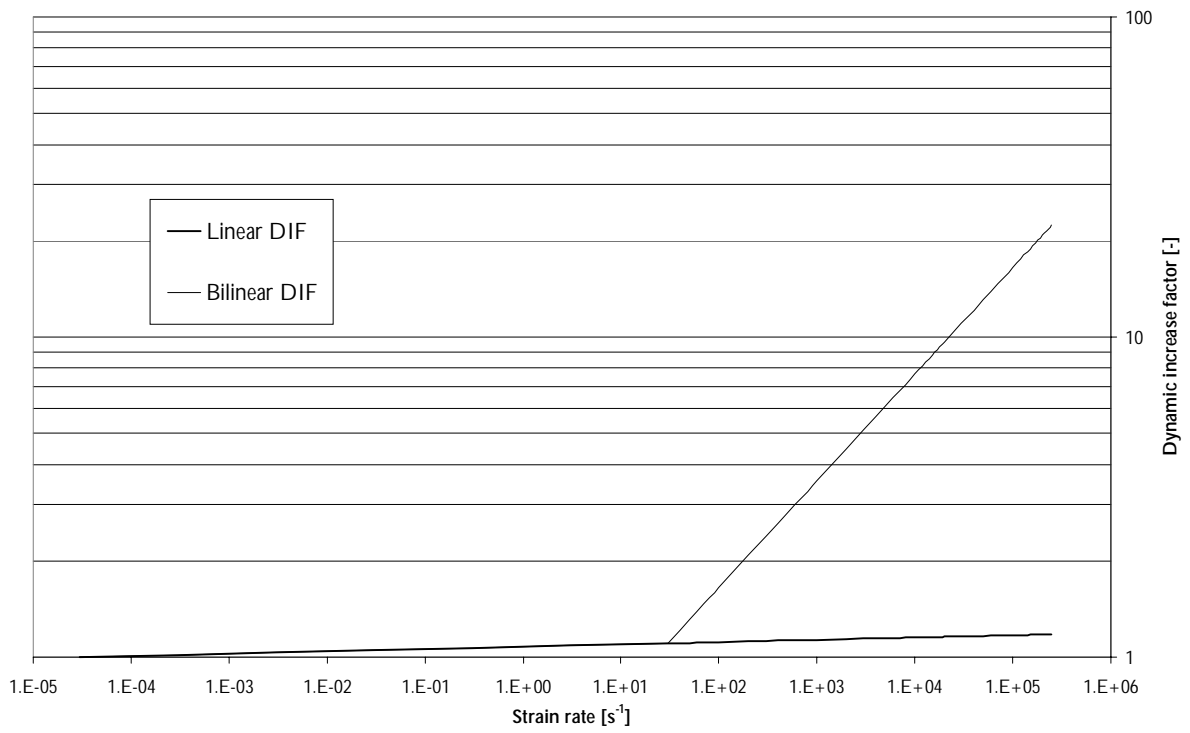


Figure 20. Strain rates in the targets impact area.



**Figure 21. Dynamic increase factor (DIF) according to [5] for uniaxial compression strength (recommended up to 300/s).**

#### 4.1 Target 1-3

The LS-INGRID input file and changes made to the created LS-DYNA keyword format input file is found in Appendix D. The mesh used for this target type is shown in Figure 22 and Figure 23. A mesh specification is given in Table 7.

The effects of dynamic strength increase of strain rate were investigated. Three curves for compressive strength enhancement were used (cf. Figure 21); no strength enhancement, linear strength enhancement and bilinear strength enhancement. The Doppler radar curves were integrated and plotted together with the measured penetration depths and the three resulting projectile velocity-displacement curves from the simulations, see Figure 24 to Figure 25. Only data up to 0.5ms was used from the Doppler radar according to discussion in chapter 2.

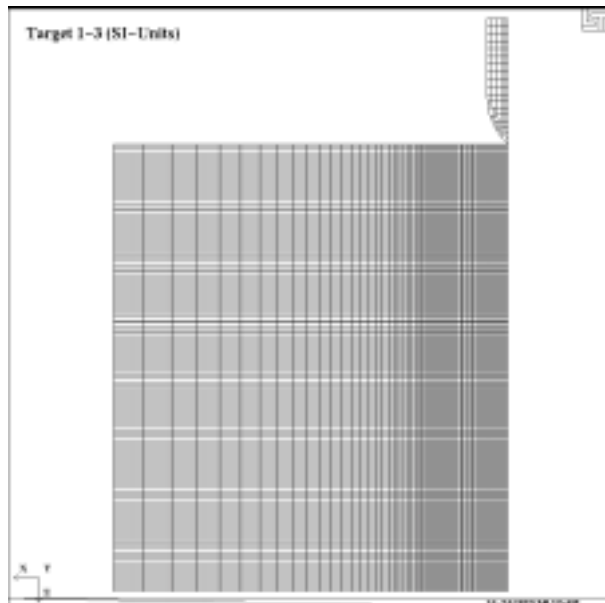


Figure 22. Mesh A in elevation view.

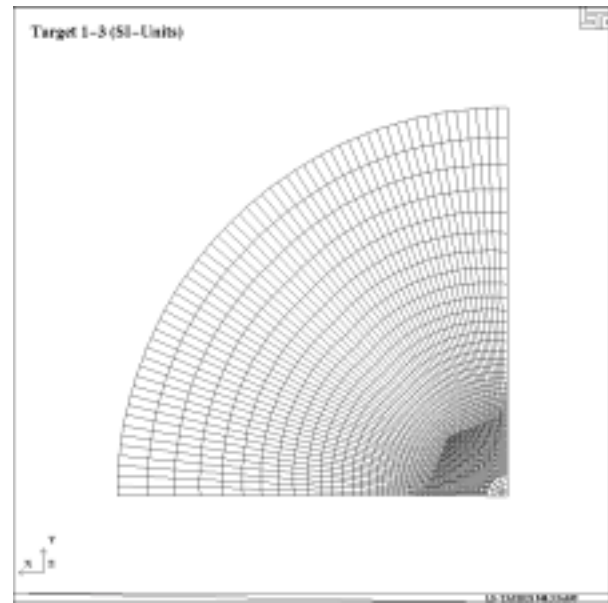


Figure 23. Mesh A in plan view.

Table 7. Mesh data for target 1-3.

Mesh	A
Characteristic element size	5mm
Nodes	419 800
Solid elements	403 200
Approx. CPU time	12 h

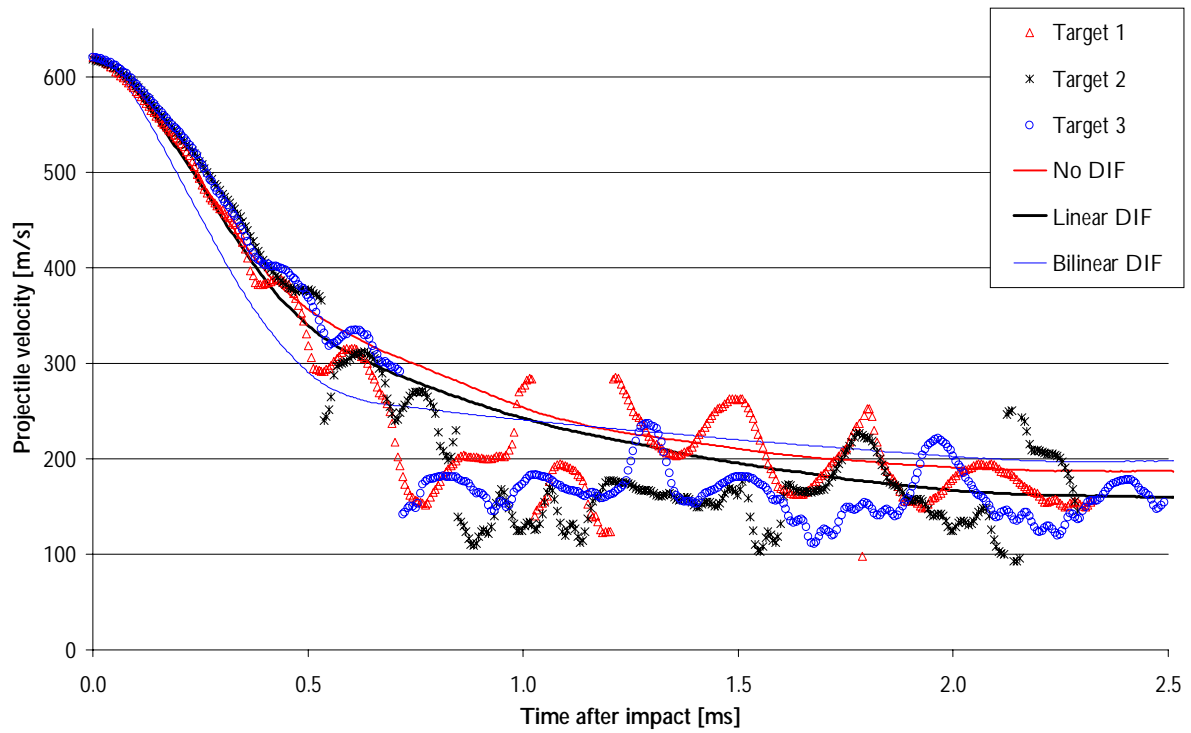


Figure 24. Comparison between numerical simulations and test data.

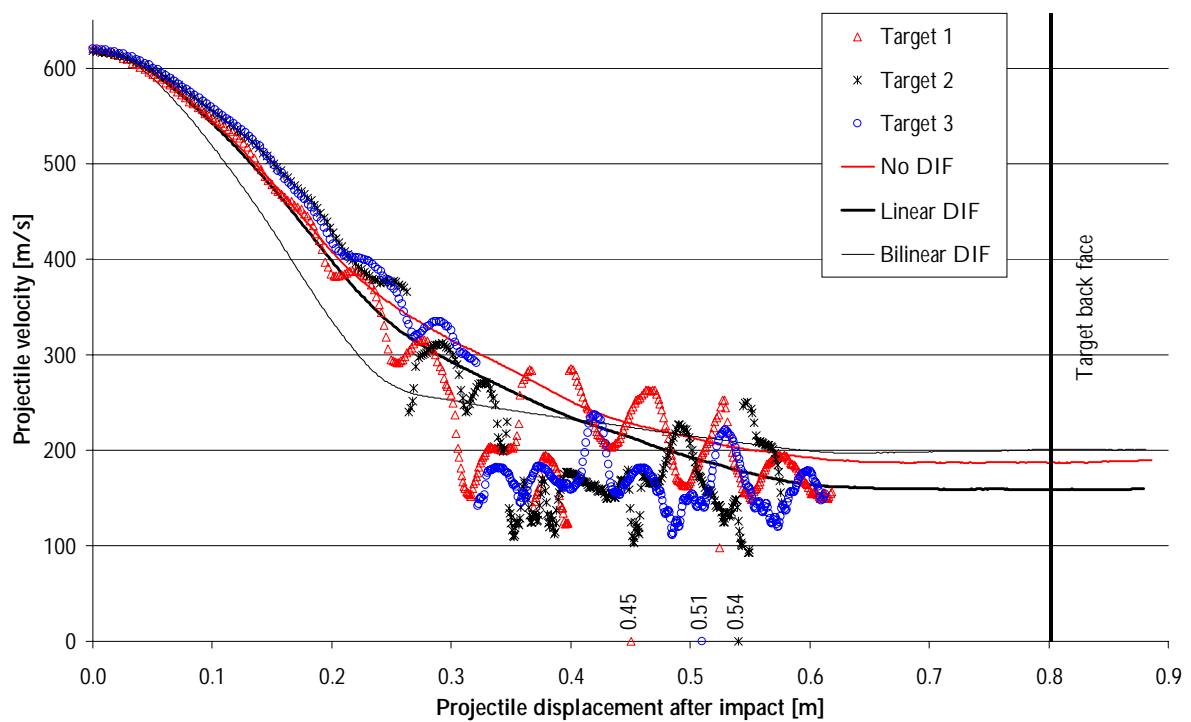
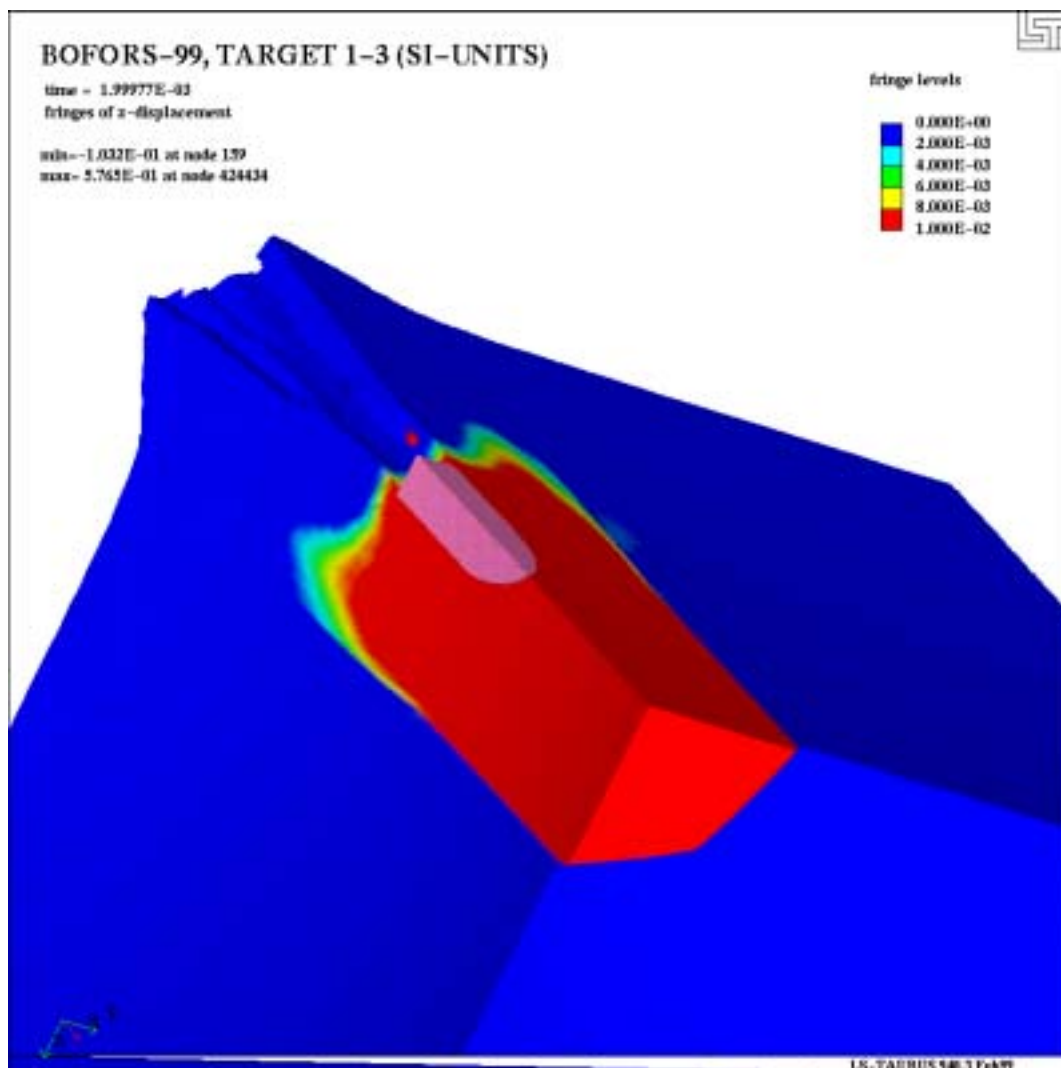


Figure 25. Comparison between numerical simulations and test data. Data points with values are depths of penetration measured after test.

Compared to data from the Doppler radar, the simulations show a higher retardation of the projectile in the beginning of the penetration phase. At a projectile displacement of about 0.25m (or 0.5ms), the retardation decreases and the decrease is more pronounced when using the bilinear DIF relation. Post-processing of the simulations show that at this moment a plug is formed in the target, see Figure 26, due to great amount of shear damage in the element size transition zone.

To investigate if the plug and thus the sudden decrease in retardation was caused by the models inability to handle different element sizes, i.e. different fracture energies, a new geometry model was constructed consisting of 5mm elements all through the target. Due to lack of memory, modelling of the whole target geometry could not be carried out. However, a smaller model with square geometry 330x330x800mm (1/4 model) and boundaries with fixed displacement and rotational constraints was created, see Figure 27 to Figure 28 and Appendix E for the LS-INGRID input file, with the specifications given in Table 8.



*Figure 26. Formation of a plug in the target due to great amount of shear damage*

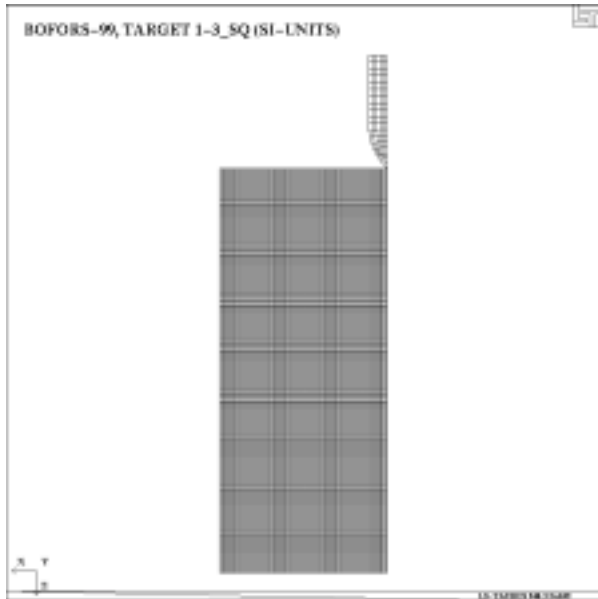


Figure 27. Mesh C in elevation view

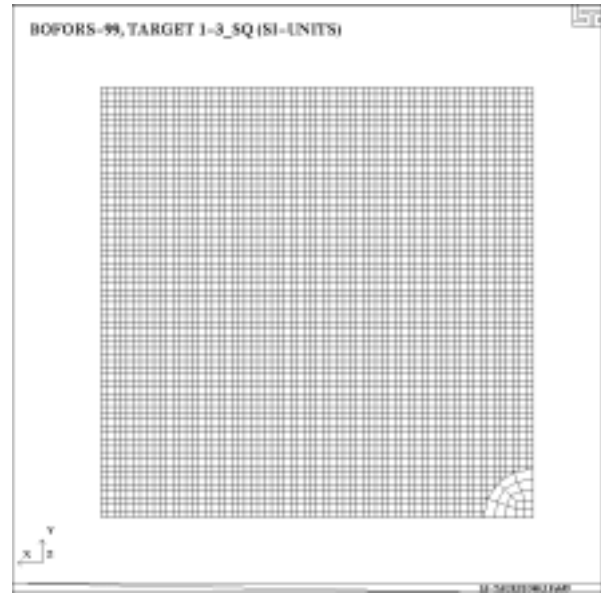


Figure 28. Mesh C in plan view

Table 8. Mesh data for square geometry target 1-3

Mesh	C
Characteristic element size	5mm
Nodes	723 125
Solid elements	697 212
Approx. CPU time	35 h

In Figure 29 and Figure 30 it is shown that when using the same element size in the whole target no plug is formed, but the sudden decrease in retardation is still there. Nevertheless, the formation of a plug leading to lower structural bearing capacity shows that there is a need to improve the model in order to make the fracture energy release objective, i.e. mesh independent. An explanation for the sudden decrease in retardation has not been found nor has been possible to conclude that this is not a real phenomenon. But, the data from the Doppler radar and the measured penetration depths indicates that this is not the case.

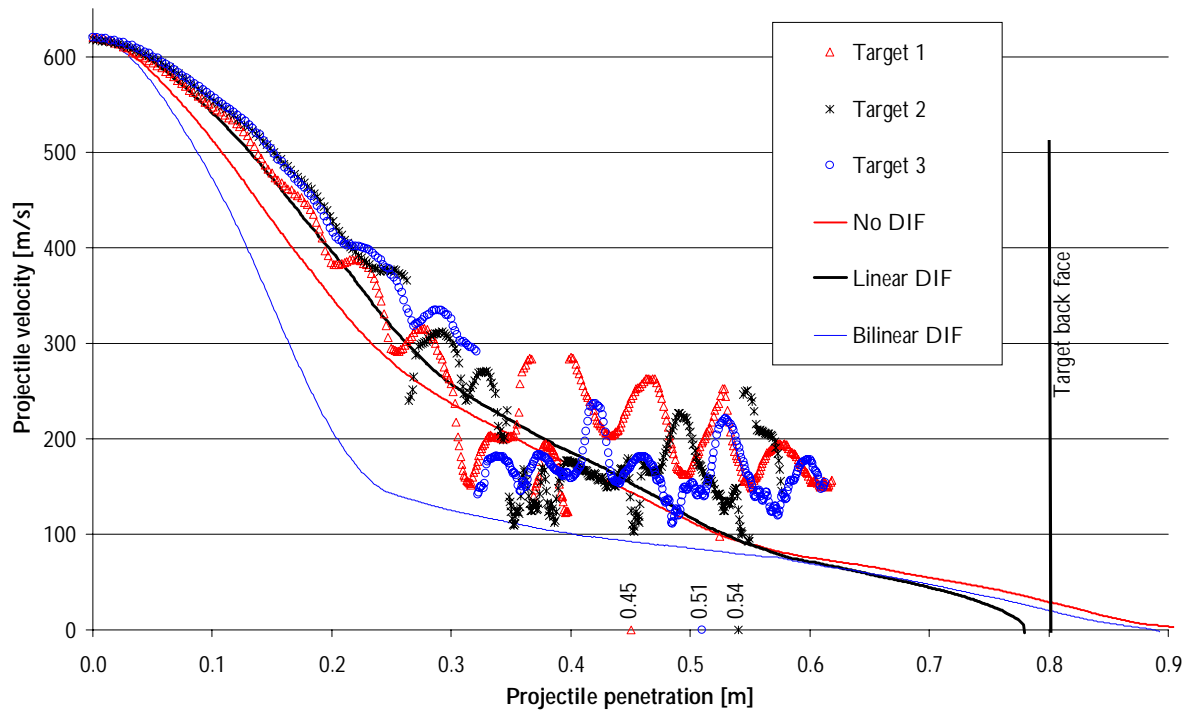


Figure 29. Comparison between numerical simulations and test data. Data points with values are depths of penetration measured after test.

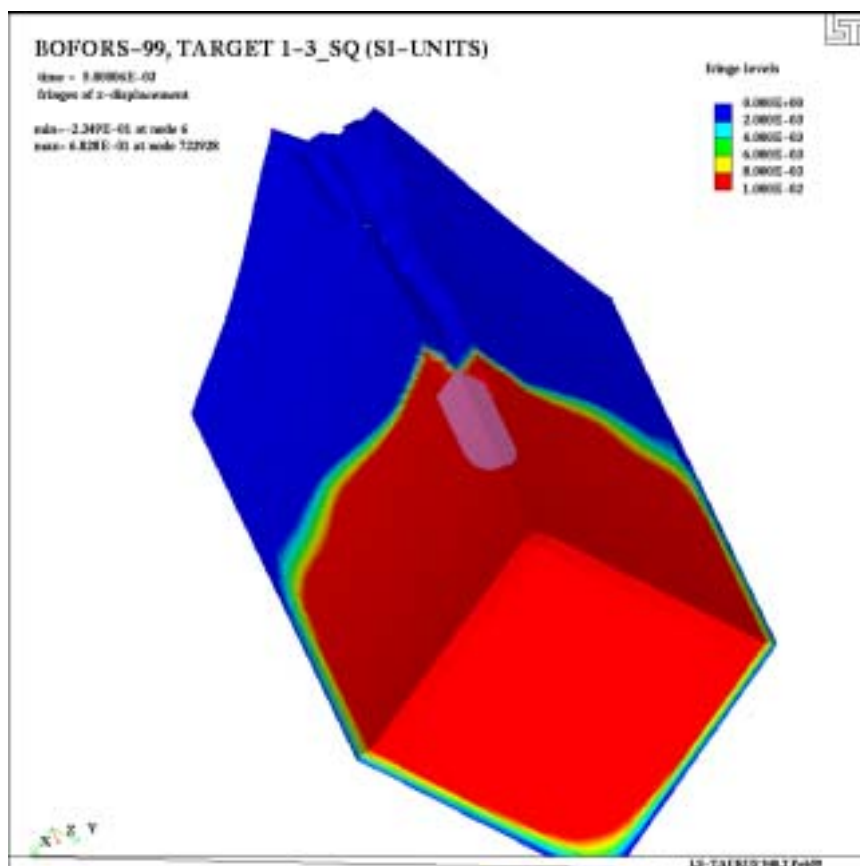


Figure 30. Longitudinal displacement for the square geometry model.

Returning now to the previous geometry model for targets 1-3, mesh A with a bilinear DIF. In Figure 31 and Figure 34 comparisons of damage are made with photos taken after the tests.



Figure 31. Post condition for front face of target 3 (shot 6).

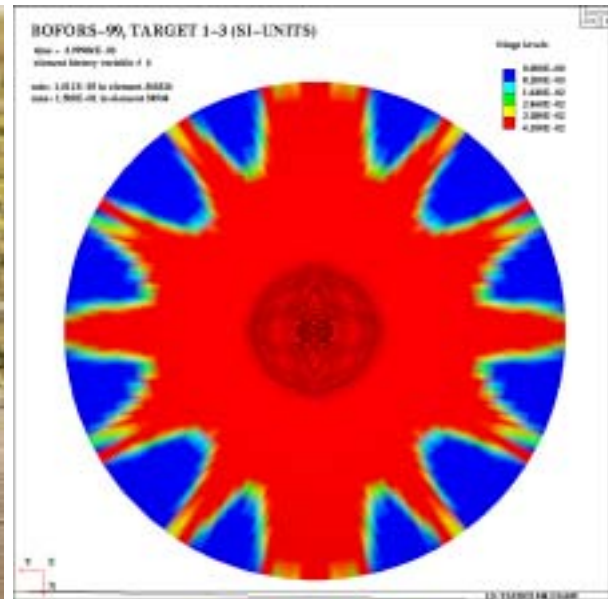


Figure 32. Damage on front face from simulation.



Figure 33. Post condition for back face of target 3 (shot 6).

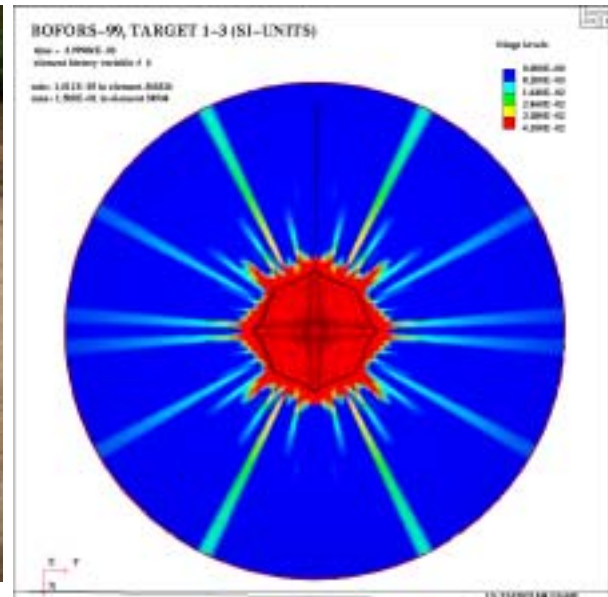


Figure 34. Damage on back face from simulation.

In Figure 35 the damage variable lambda is plotted on the symmetry plane. According to this figure the target is almost completely damaged, which is not consistent with the test results.

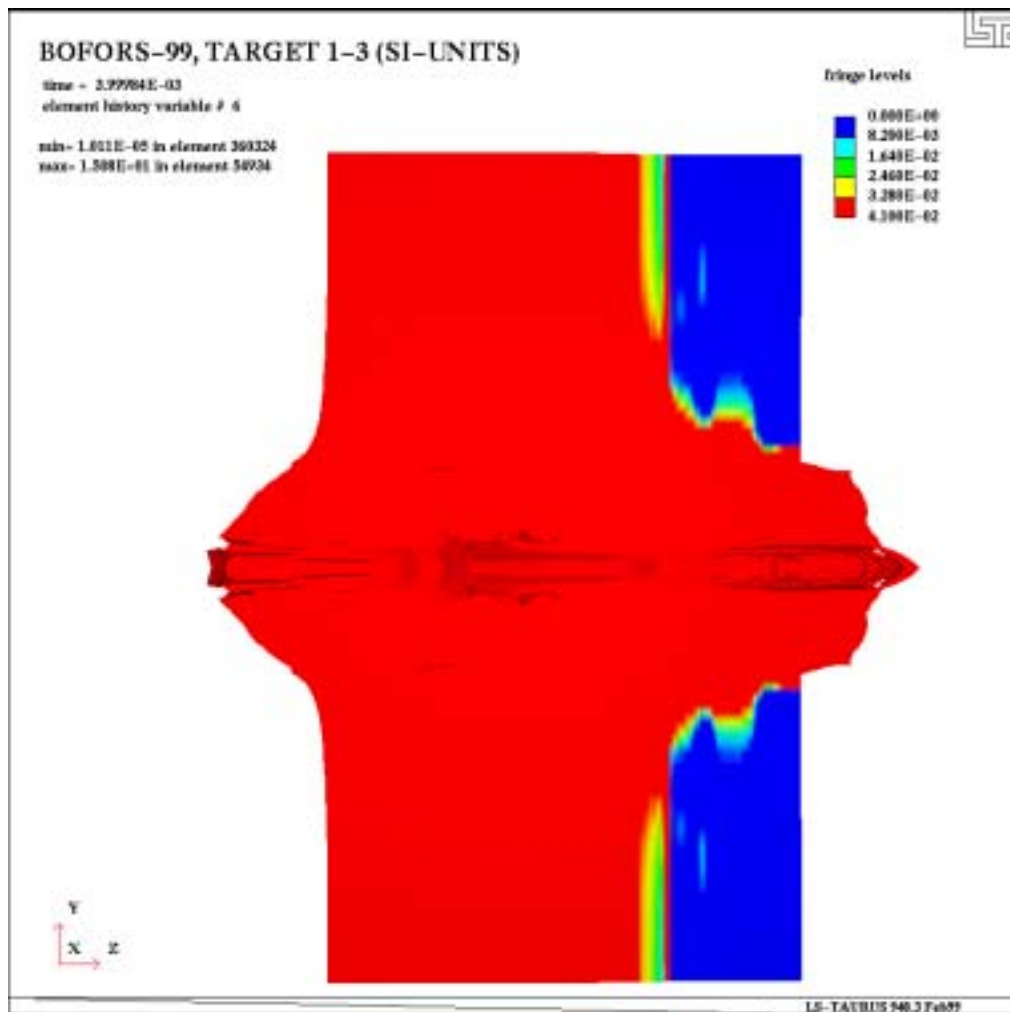


Figure 35. Damage in target, side view.

## 4.2 Target 4-6

The LS-INGRID input file and changes made to the created LS-DYNA keyword format input file is found in Appendix C. The mesh used for this target is shown in Figure 36 and Figure 37 and in Table 9 mesh specifications are given.

First, the element size dependency was investigated using no DIF relationship. The results are presented in Figure 38 where it is obvious that the fracture energy release is not objective, i.e. adjusting the parameters  $b_1$ ,  $b_2$ , and  $b_3$  does not eliminate mesh dependency. The elements outside the impacting area that are bigger than 5mm and 7.5mm respectively might also influence the result. For larger elements, the energy release is lower giving a higher residual velocity. This is consistent with the observed results. For erosion shear strain values over 0.9 the mesh becomes heavily distorted, why this value is taken as maximum.

The influence of dynamic friction (no DIF) was also investigated, see Figure 39. Obviously, the friction has none or little effect on the result. This is due to the small area of contact between the projectile and the target, see Figure 40. At the nose, the elements are deleted according to the erosion criteria and towards the rear of the projectile, the whole in the target has a conical shape leaving a void between projectile and target.

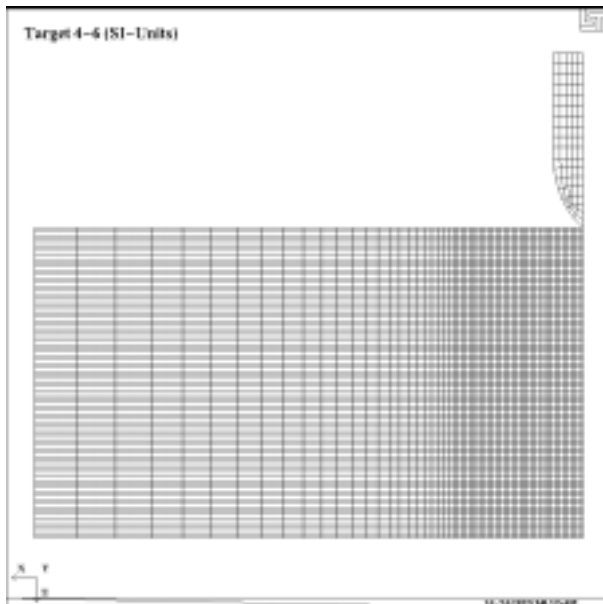


Figure 36. Mesh A in elevation view.

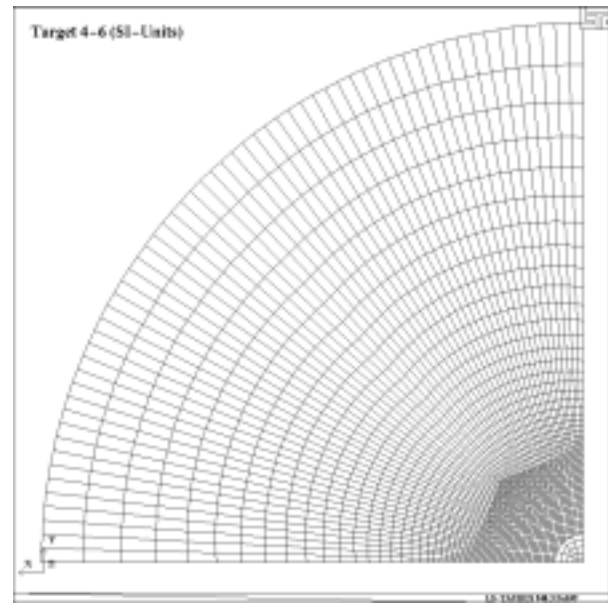


Figure 37. Mesh A in plan view.

Table 9. Mesh data for targets 4-6.

Mesh	A	B
Characteristic element size	5mm	7.5mm
Nodes	211 160	51 212
Solid elements	201 600	47 488
Approx. CPU time	3 hours	1 hour

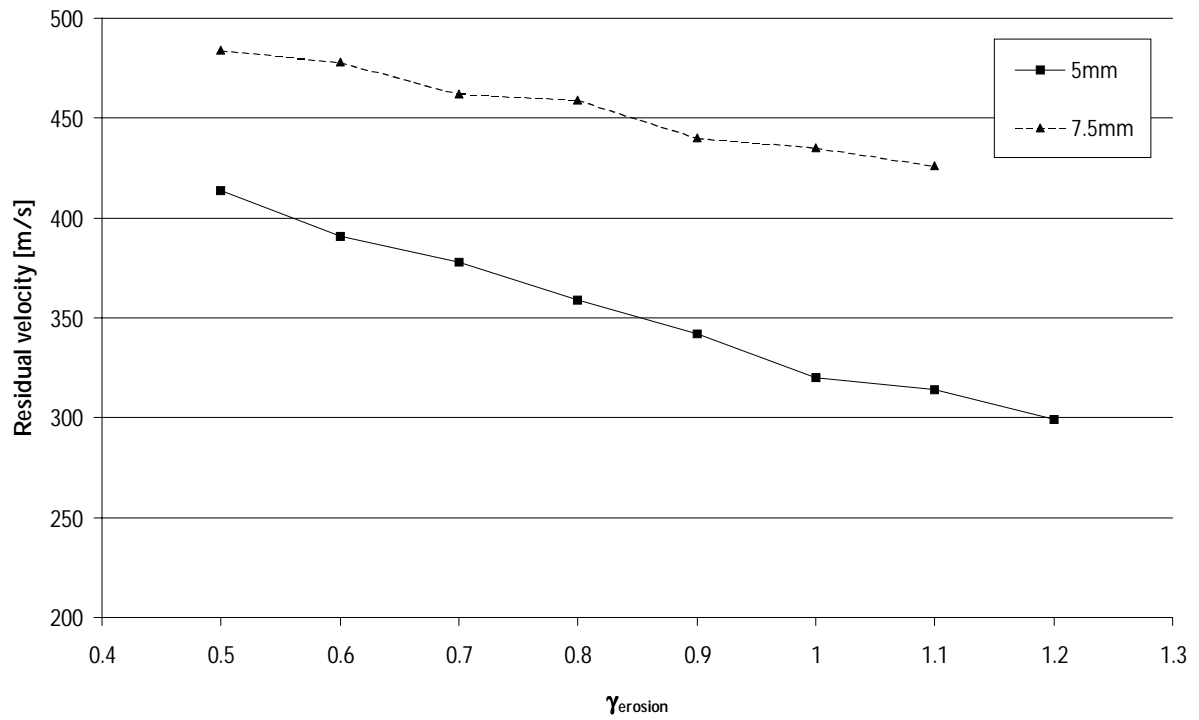


Figure 38. Influence of mesh element size and erosion shear strain on residual velocity (no DIF).

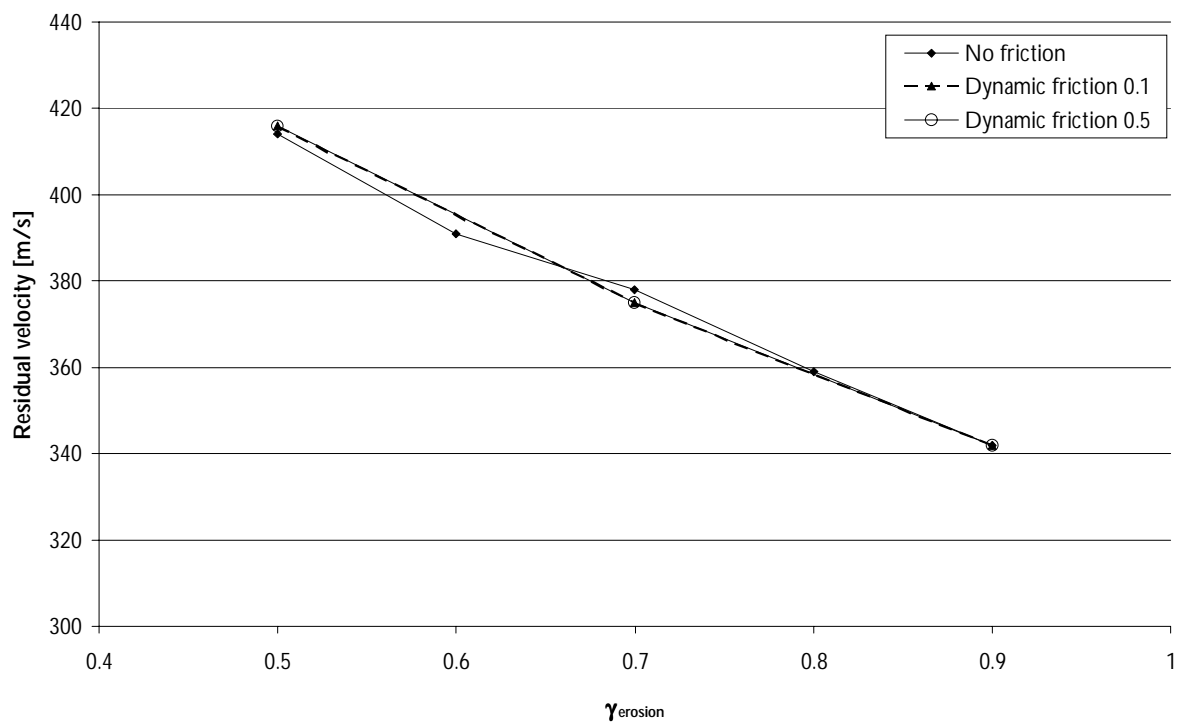
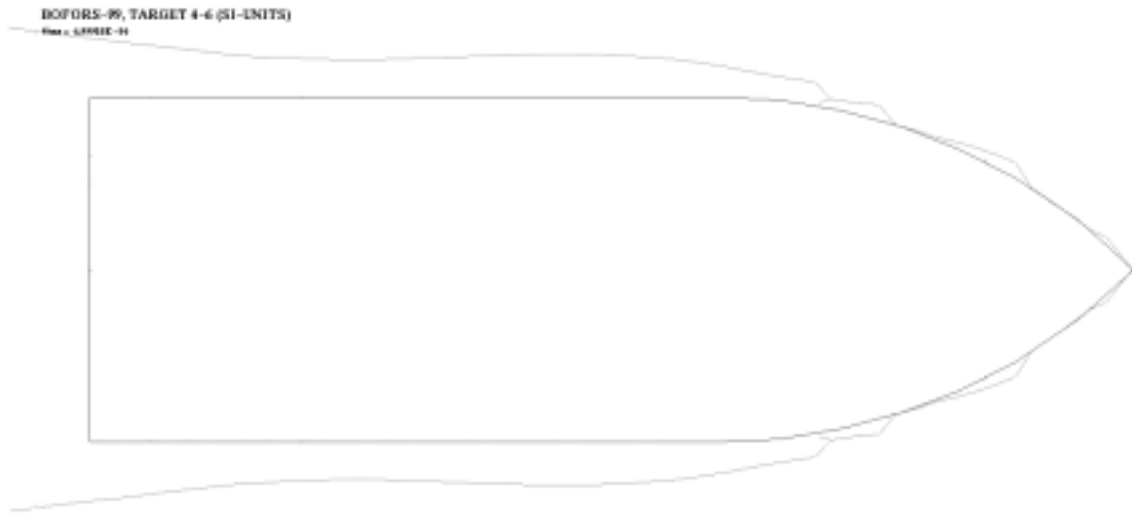


Figure 39. Influence of dynamic friction on residual velocity (no DIF).



**Figure 40. Contact between projectile and target**

The strain rate dependency was investigated using two curves, see Figure 41, for dynamic increase of the target's compressive strength. The computations were carried out with an erosion shear strain of 0.9.

Integrating the Doppler radar curve and plotting it against the projectile velocity shows the projectile trajectory through the target, see Figure 42.

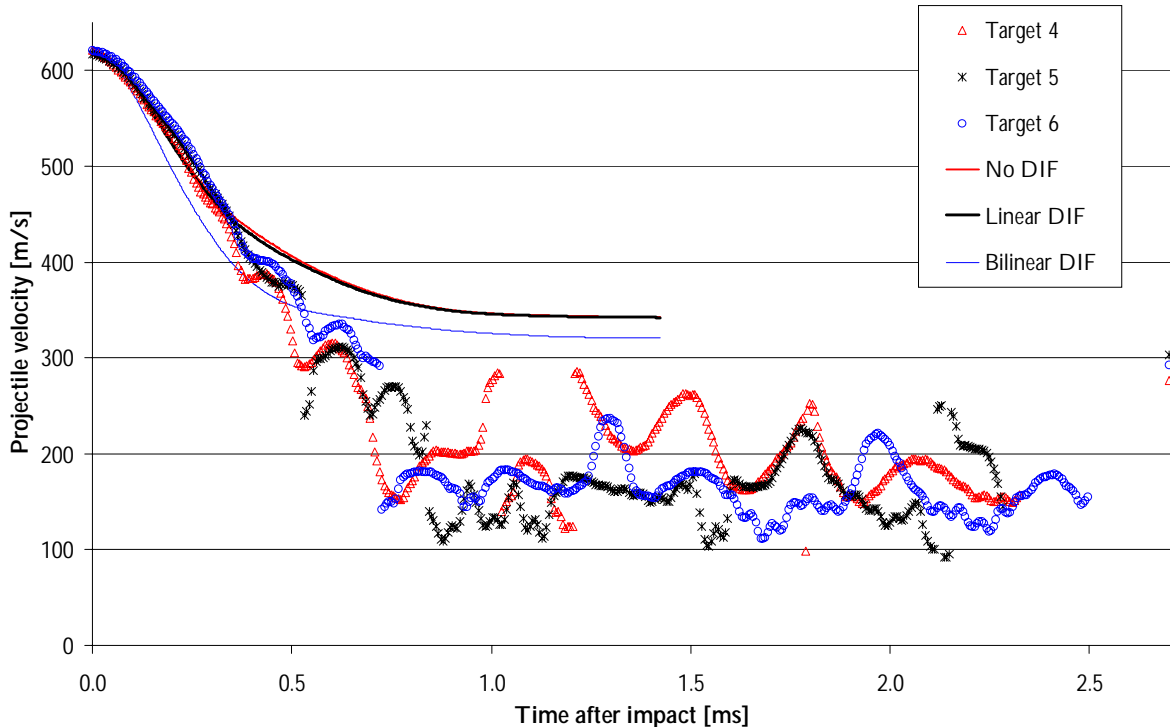


**Figure 41. Comparison between numerical simulations and test data.**

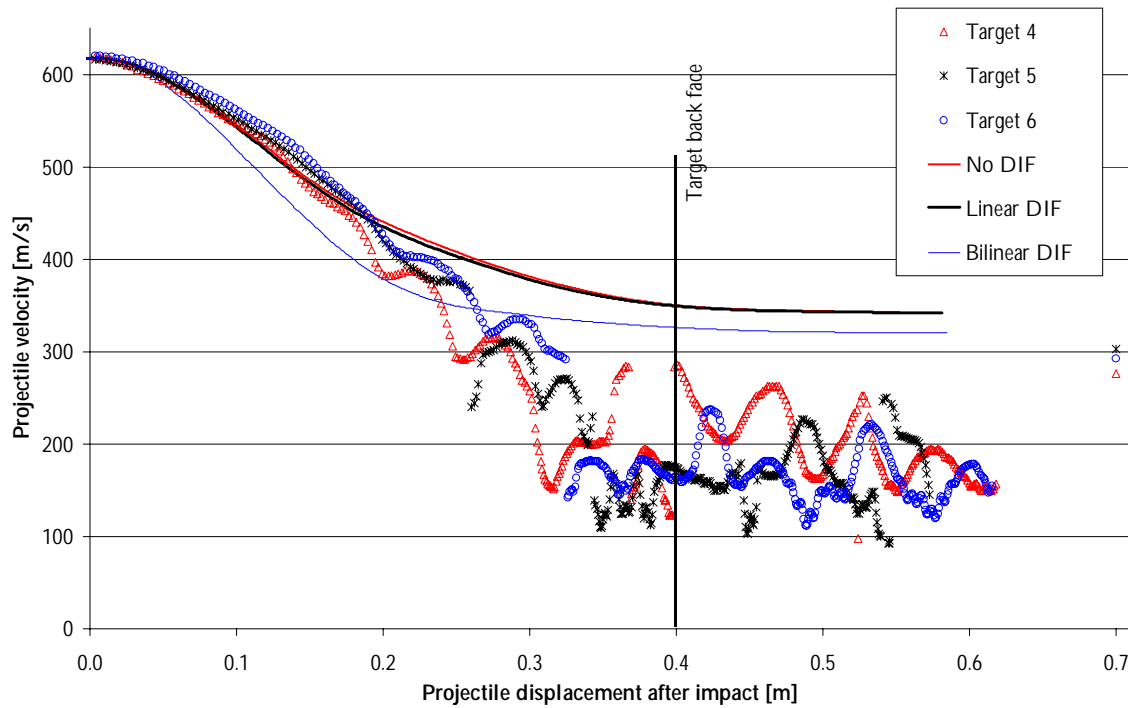


**Figure 42. Comparison between numerical simulations and test data. Data points with values are taken from high-speed videos.**

In this simulation, as for targets 1-3, a plug is formed in the transition zone between different element sizes, decreasing the structural bearing capacity, see Figure 43. However, the effect of this phenomenon seems less important because of the smooth retardation.

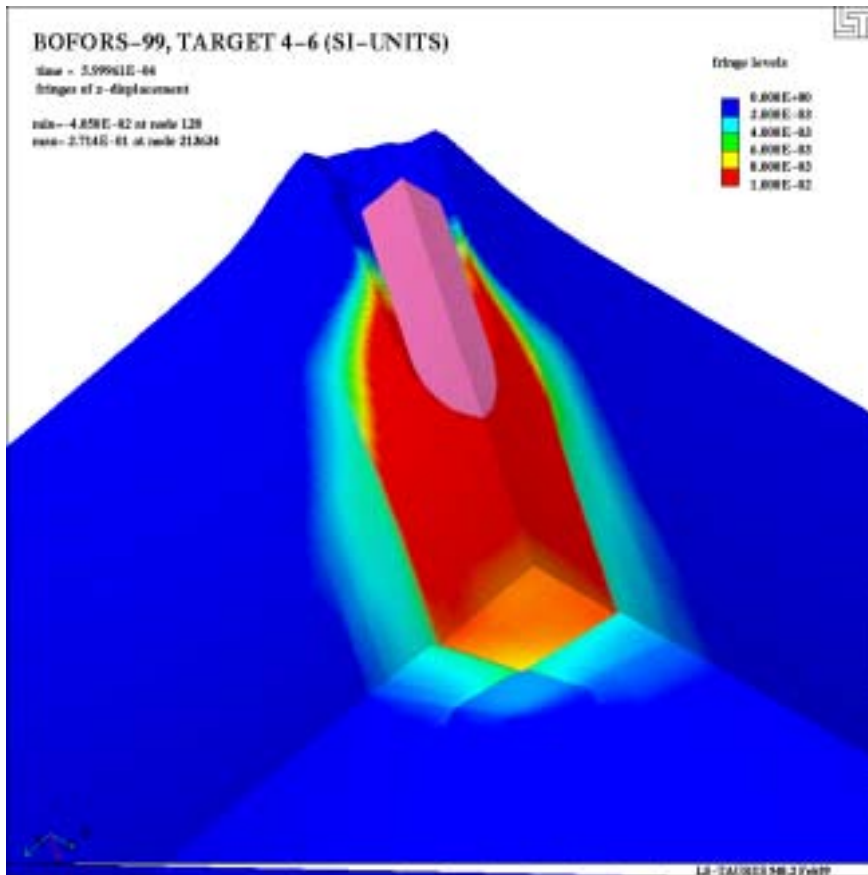


Figure 43. Longitudinal displacement for target 4-6, element size 5mm and no DIF.

Comparisons of photos from the tests with plots of the damage parameter lambda from the simulation (bilinear DIF), see Figure 44 to Figure 47, reveals almost the same damage pattern as for target 1-3.



Figure 44. Post condition for front face of target 5 (shot 2).

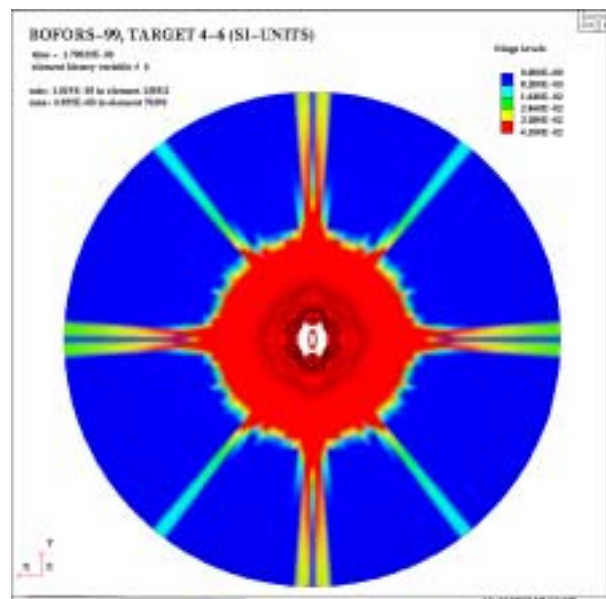


Figure 45. Damage on front face from simulation.



Figure 46. Post condition for back face of target 5 (shot 2).

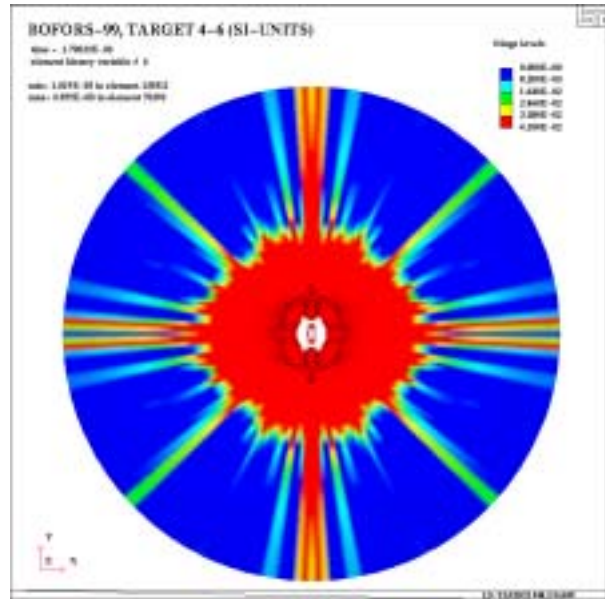


Figure 47. Damage on back face from simulation.

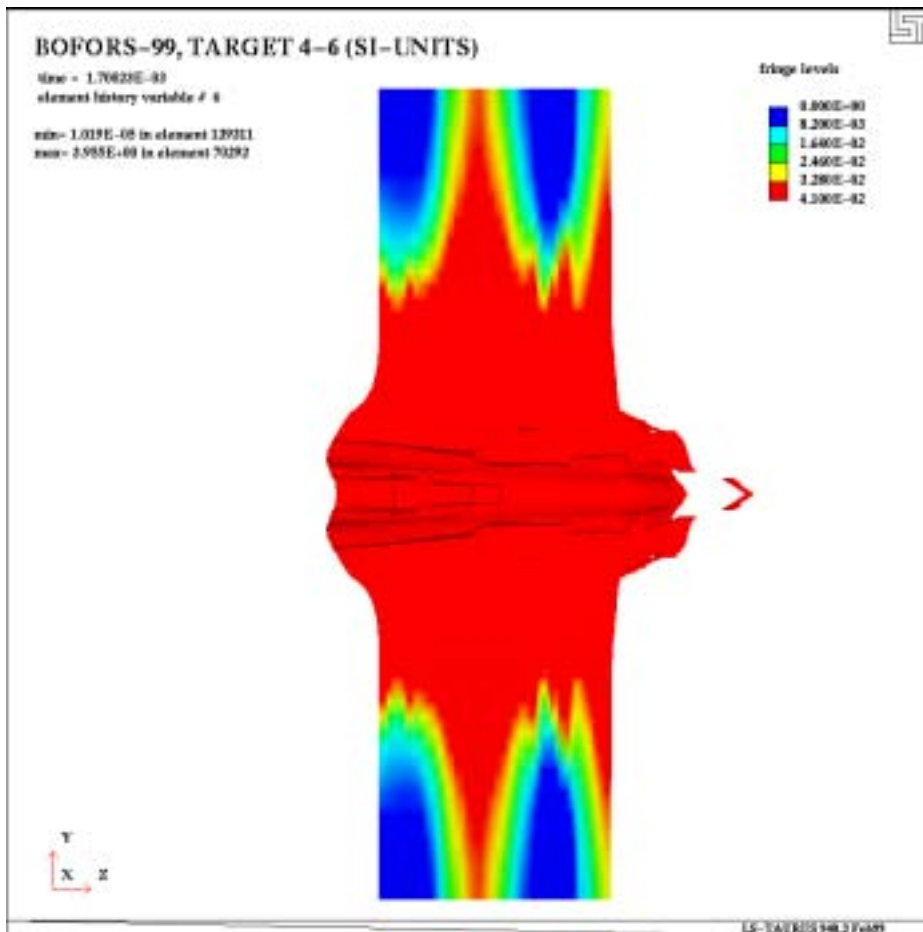


Figure 48. Damage in target, side view.

### 4.3 Target 7-9

The LS-INGRID input file and changes made to the created LS-DYNA keyword format input file is found in Appendix C. Due to difficulties with connecting the reinforcement to the target mesh these tests were modelled using square geometry, see Figure 49 to Figure 52. The reinforcement was modelled using truss elements and the nodes were tied to the corresponding nodes for the target brick elements. In table Table 10 mesh specifications are given.

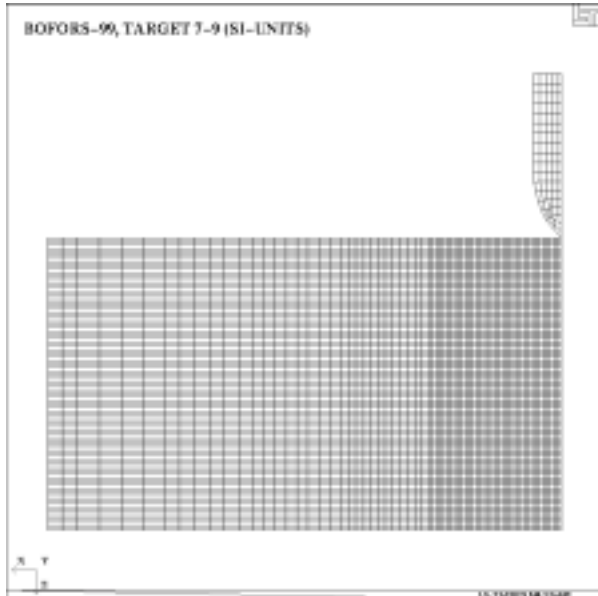


Figure 49. Mesh A in elevation view.

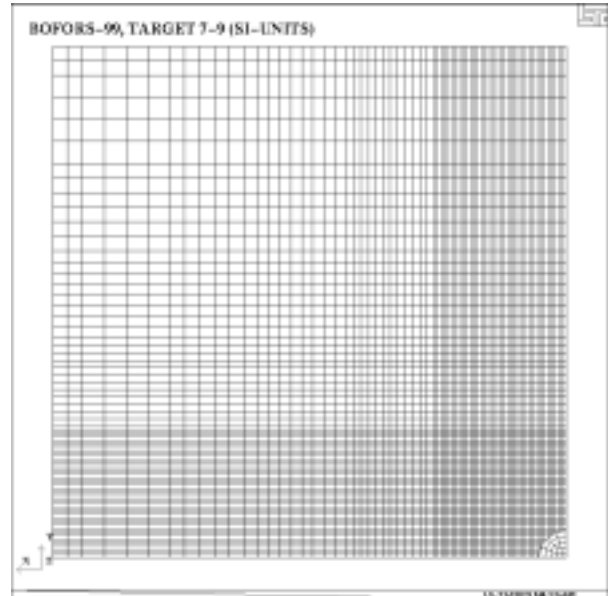


Figure 50. Mesh A in plan view.



Figure 51. Elevation view of reinforcement cage.

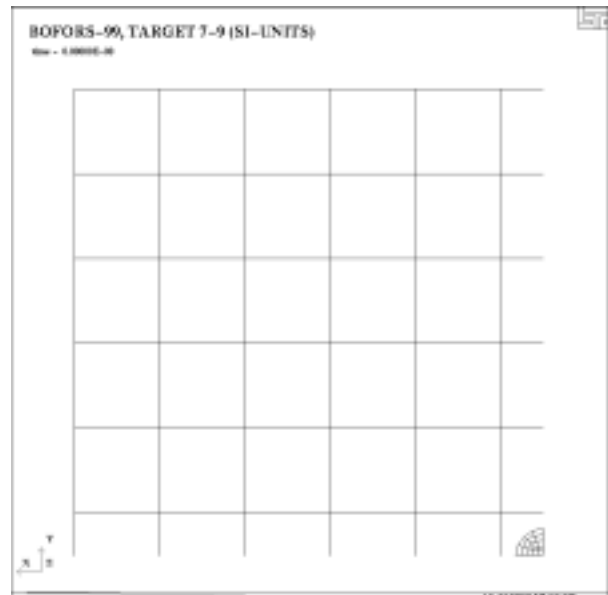
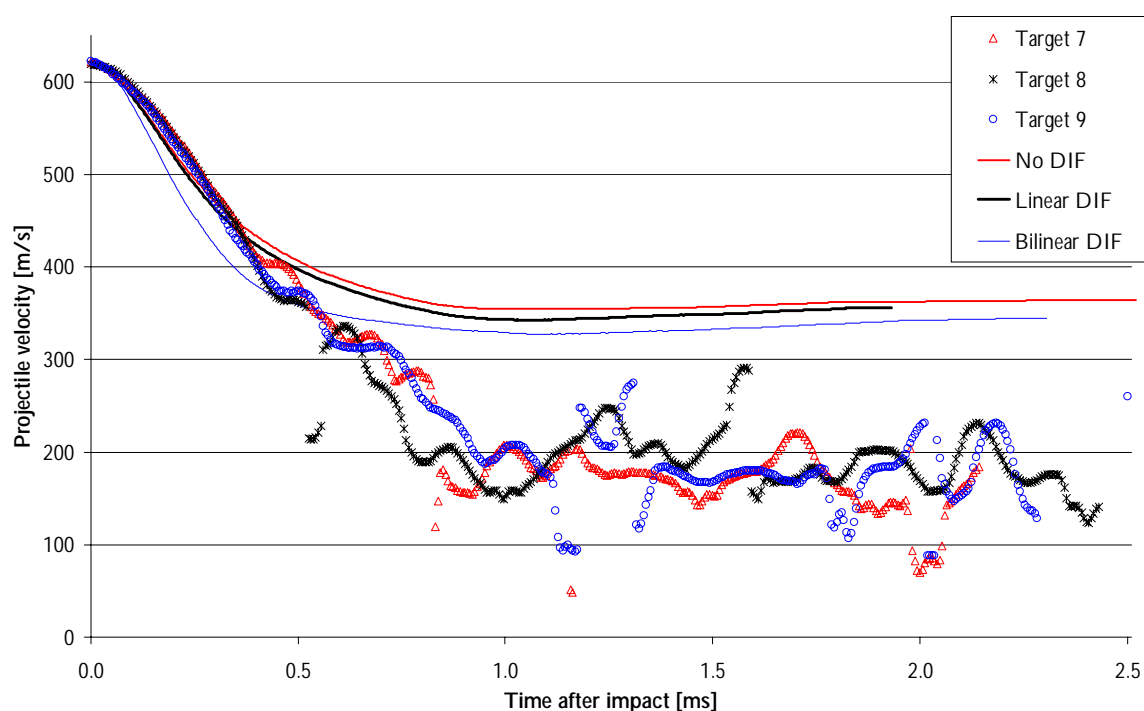


Figure 52. Plan view of reinforcement cage.

**Table 10. Mesh data for targets 7-9.**

Mesh	A
Characteristic element size	5mm
Nodes	392 792
Solid elements	369 920
Truss elements	7 092
Approx. CPU time	7 h

The strain rate dependency was investigated with an erosion shear strain of 0.9. Integrating the curves in Figure 53 and plotting it against the projectile velocity shows the projectile trajectory through the target, see Figure 54. In Figure 55, a damage plot is given showing the formation of a plug .



**Figure 53. Influence of dynamic increase factor (DIF) on projectile retardation.**

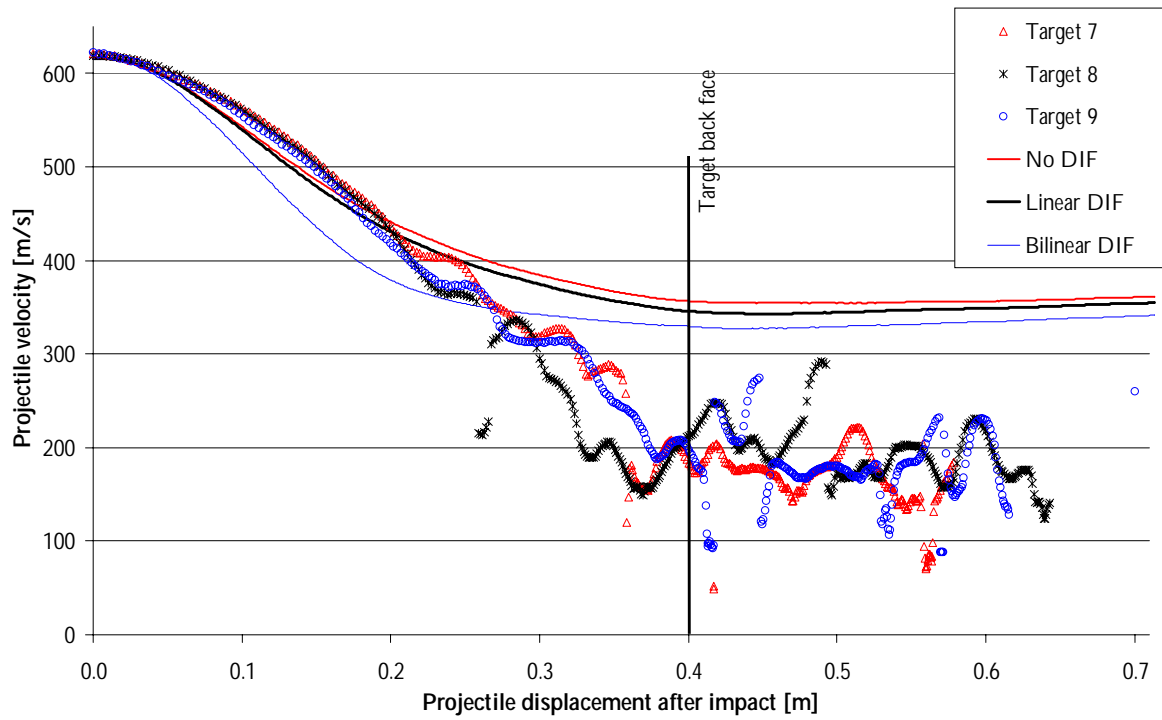


Figure 54. Influence of dynamic increase factor (DIF) on projectile retardation.

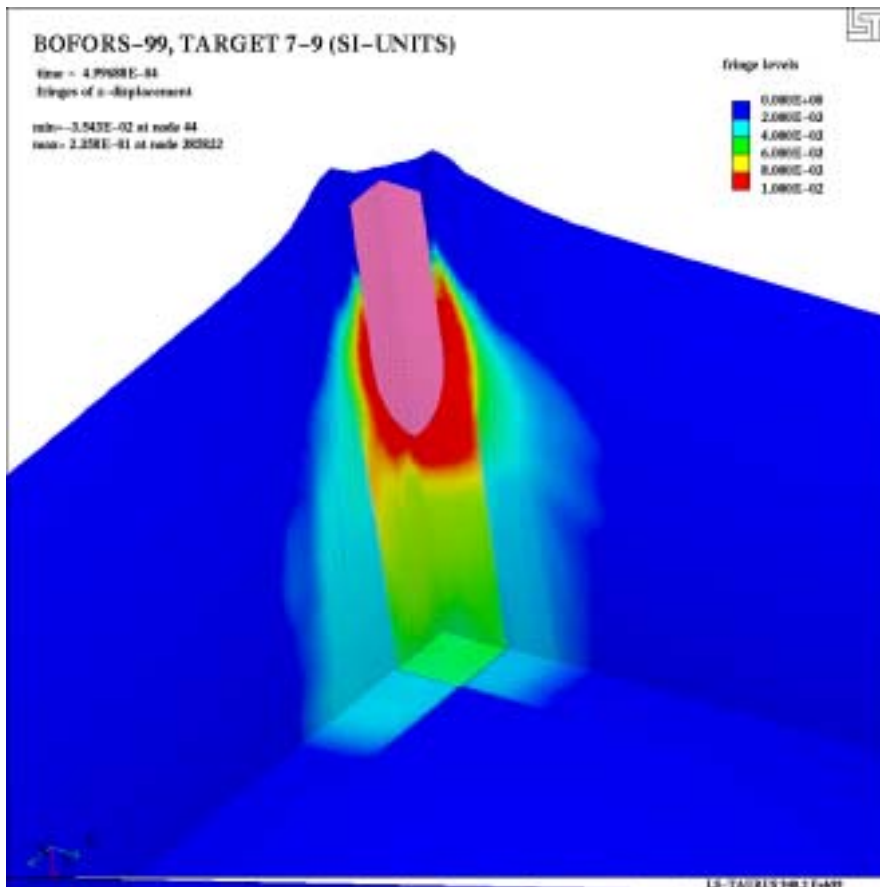


Figure 55. Longitudinal displacement for target 7-9, element size 5mm and no DIF.

In Figure 56 to Figure 59 comparisons of the damage parameter lambda are made with photos taken after the tests. In Figure 61 to Figure 62 a comparison is made for reinforcement displacement at the target back face after perforation.



Figure 56. Post condition for front face of target 7 (shot 7).

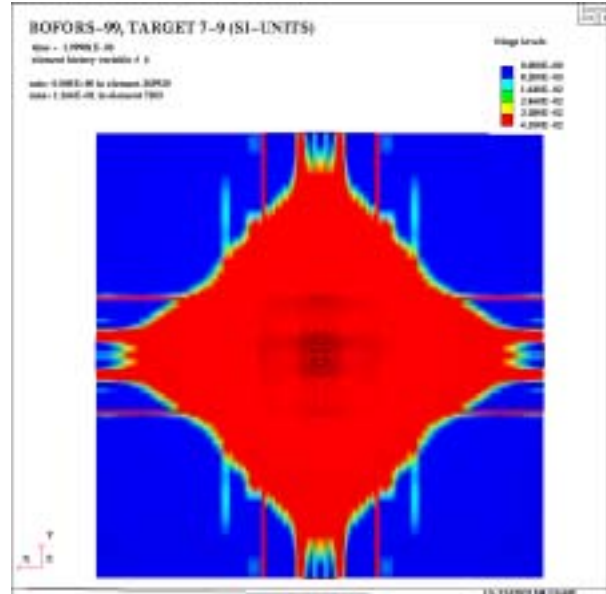


Figure 57. Damage on front face from simulation (bilinear DIF).



Figure 58. Post condition for back face of target 9 (shot 9).

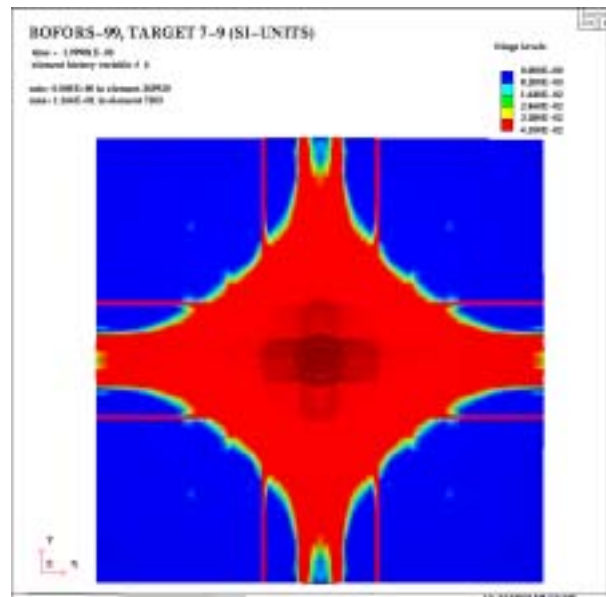


Figure 59. Damage on back face from simulation (bilinear DIF).

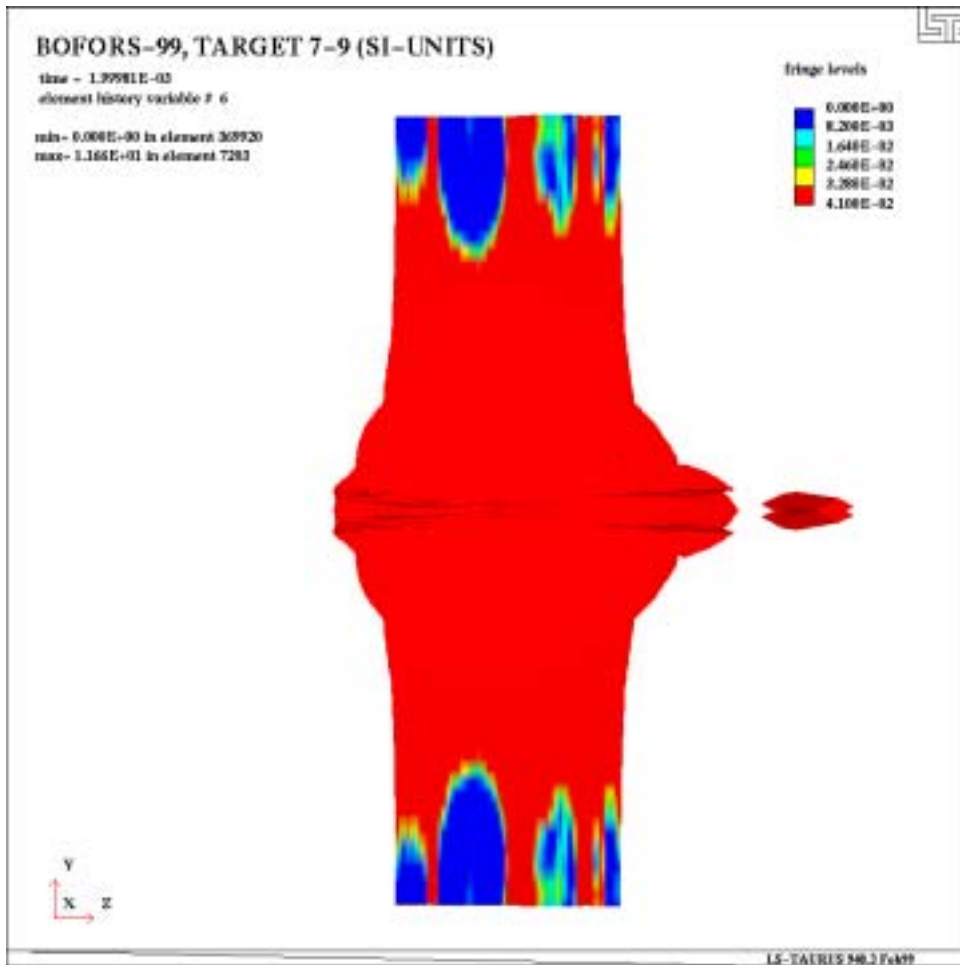


Figure 60. Damage in target, side view (bilinear DIF).



Figure 61. Post condition for reinforcement at back face of target 7 (shot 7).

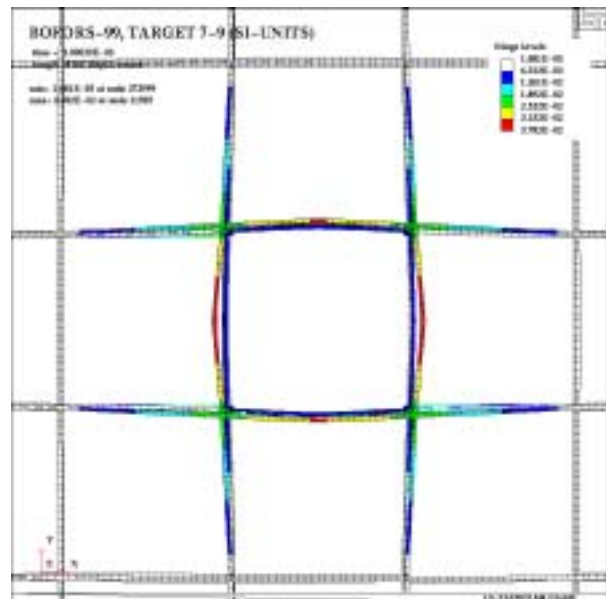


Figure 62. Post condition for reinforcement at back face of target 7 from simulation.

## 5 SUMMARY

Numerical simulations of penetration and perforation tests of high strength concrete have been carried out. The problem was modelled in LS-DYNA and solved using Lagrangian technique. Influence of strength enhancement based on strain rate, numerical erosion criteria, friction between target and projectile and mesh dependency has been investigated.

Results from the computations were compared to test data on the projectile trajectory and photos showing the damaged targets. For perforation, the projectile's trajectory was derived from Doppler radar and high-speed photos. In the case of penetration, the projectile's trajectory was derived from Doppler radar and measurements on depth of penetration.

The simulations show good agreement with test data for perforation. For penetration, the results are not satisfying since in the simulations the projectile perforates the target, which was not the case for the tests, see Table 11.

*Table 11. Comparison of results from test and numerical simulations.*

Target number	Projectile impact velocity [m/s]	Test		Numerical simulation	
		Depth of penetration [mm]	Projectile residual velocity [m/s]	Depth of penetration [mm]	Projectile residual velocity [m/s]
1-3	616	500	-	-	200
4-6	617	-	291	-	320
7-9	616	-	260	-	330

During the work with the simulations, problems have been encountered in the following areas.

- Material type 72

The target material model does not allow different element sizes to be used in one material definition. The damage curve is fitted to one specific element size and when using different sizes of elements one do not get the right energy release. Future improvements of the model should include regularisation of the fracture so that the fracture energy release becomes objective, i.e. mesh independent. This problem with the fracture energy release seems to be a possible explanation for the great amounts of shear damage in the element transition zones. The authors of the material model have improved the model since the first release, which is the one implemented in LS-DYNA. In Appendix B improvements made in a more recent release, release II, of the model are listed.

- Numerical erosion

In LS-DYNA, there are six different types of erosion criteria, which can be used, with all material types and one-point integrated solid elements. The value on the erosion criteria has great influence on the results but the determination of the erosion criteria parameters is difficult, as the mesh becomes much distorted at large values. This problem suggests that another solution technique should be used, for example Euler or smooth particle hydrodynamic (SPH). A new erosion criterion should also be added to this particular material type, based on the modified effective plastic strain parameter lambda. This would give the possibility to ensure on self that all fracture energy had been released before eroding, or deleting, the element.

- Interaction between concrete and reinforcement

With concrete to reinforcement mass ratio of 6%, one cannot use a smeared approach to model the rebars and stirrups. In this report, truss-elements were used, but this is not sufficient to take into account the confinement contributed by the reinforcement. The rebars should be modelled as either solid elements with a concrete-rebar interface or using beam elements and a slip model. For beam elements there is a possibility to model slip in LS-DYNA with an option called 1-d slide line, which haven't been applied to this problem.

- Dynamic increase factor (DIF)

When enhancing the material strength using a DIF relation the structural response changes in the beginning of the penetration phase, the retardation of the projectile increases. However, for all the cases considered here this effect seems to last only to half the targets depth and we almost get a converging residual velocity for all three DIF relations. For targets 1-3, where the projectile should come to rest in the target according to the test, a extrapolation of the initial retardation phase points to the measured depths of penetration. An explanation for what causes the pronounced bend on the projectiles penetration path, see for example Figure 25, has not been found in this report.

## REFERENCES

1. LSTC (1999). *LS-DYNA keyword user's manual, non-linear dynamic analysis of structures, version 950*. Livermore Software Technology Corporation, LSTC report.
2. Malvar L J, Crawford J E, Wesevich J W, Simons D: *A Plasticity Concrete Material Model for Hydrocodes*. International Journal of Impact Engineering, Vol. 19, Nos. 9-10, pp 847-873. Elsevier Science Ltd. 1997.
3. LSTC (1990). *LS-TAURUS: An interactive post-processor for the analysis codes LS-NIKE3D, LS-DYNA3D and TOPAZ3D*. Livermore Software Technology Corporation.
4. AB Svensk Byggtjänst (1997): *Betonghandboken Material, utgåva 2*. ISBN 91-7332-799-9.
5. CEB (1993): *CEB-FIP Model Code 1990, Design Code*. ISBN 0-7277-1696-4. Thomas Telford publishing.
6. LSTC (1998). *LS-INGRID: A pre-processor and three-dimensional mesh generator for the programs LS-DYNA, LS-NIKE3D and TOPAZ3D, version 3.5*. Livermore Software Technology Corporation, LSTC report.
7. O'Carroll, Cathy (1999): Advances for modelling of geological materials. *Material Test Procedures in Support of Dynamic Material Modelling*. Defence Research Establishment, Report FOA-R- -99-01227-311- -SE. ISSN 1104-9154.

# APPENDICES

## Appendix A

The following plots show the frequency intensity from the Doppler radar and a predicted projectile path. For each target two plots are presented, the first showing all data and the second only for the penetration phase.

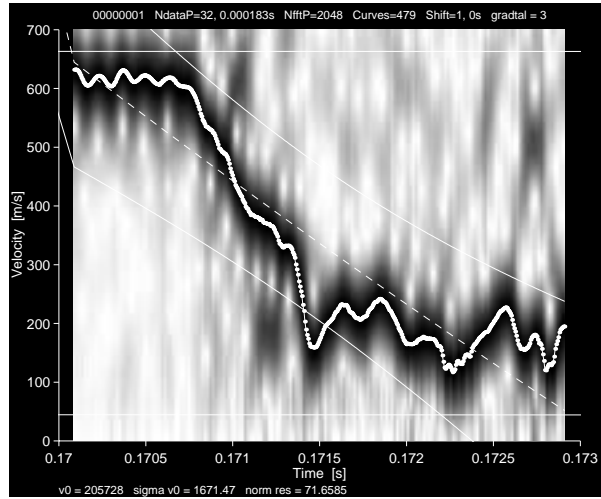
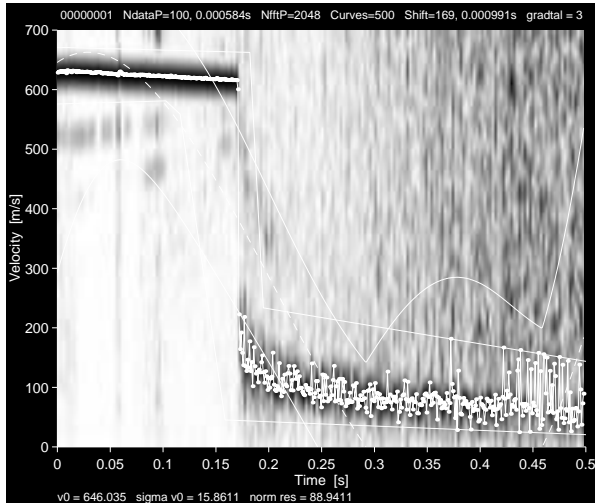


Figure 63. Doppler radar data for target 1

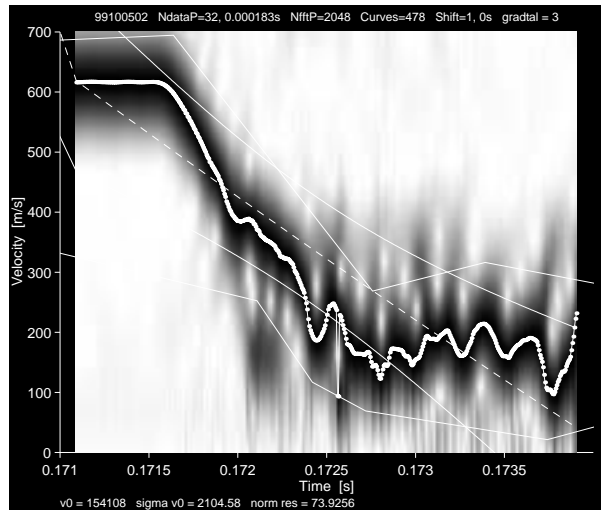
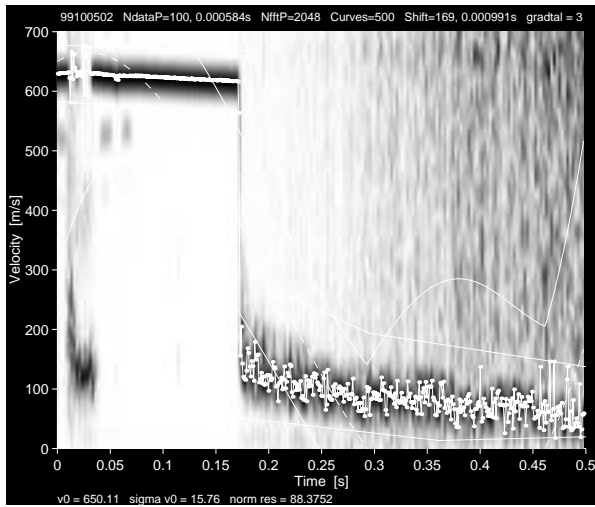


Figure 64. Doppler radar data for target 2

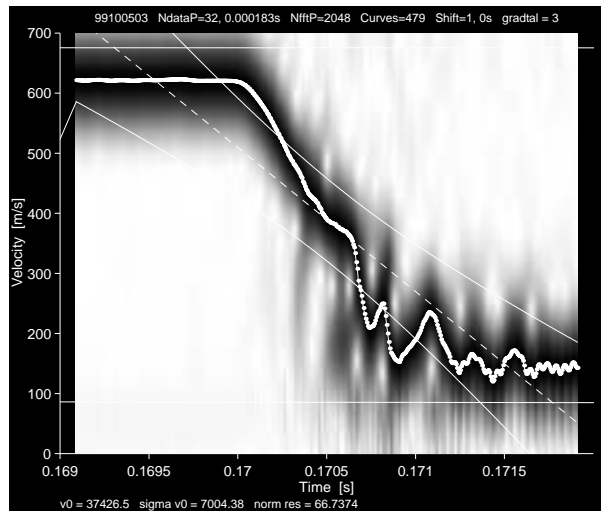
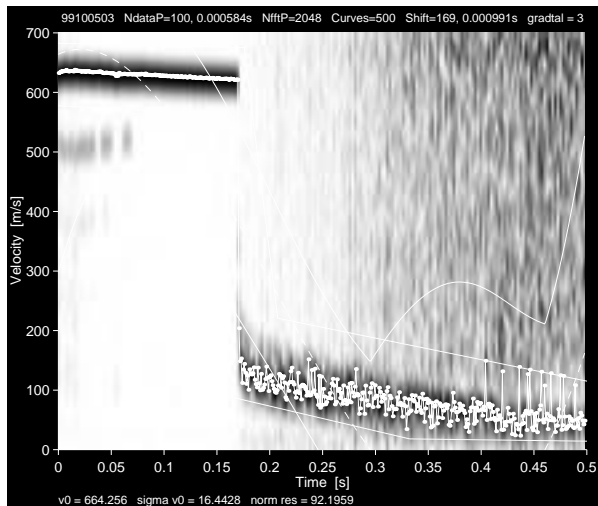


Figure 65. Doppler radar data for target 3

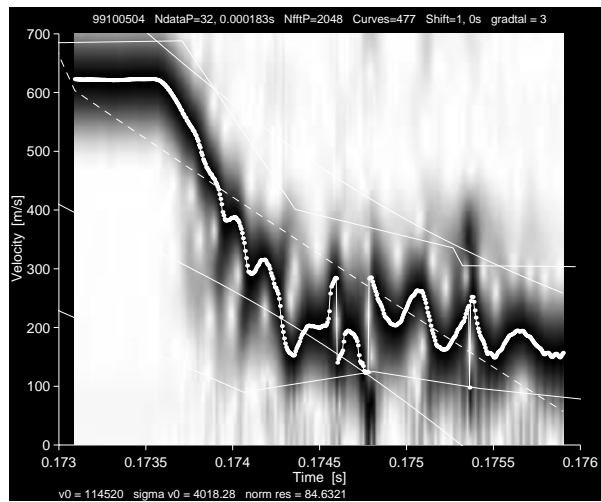
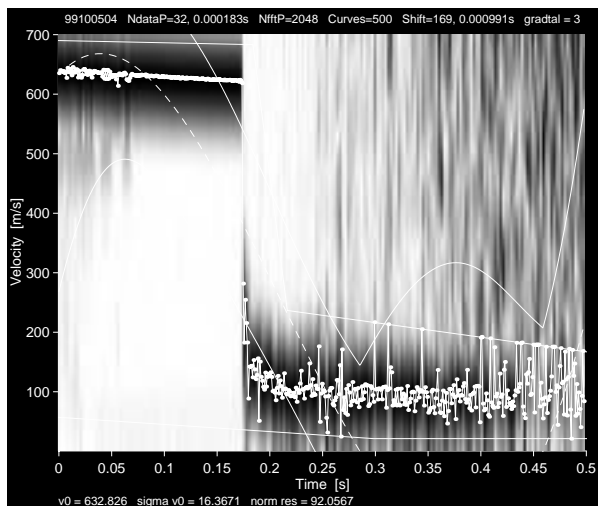


Figure 66. Doppler radar data for target 4

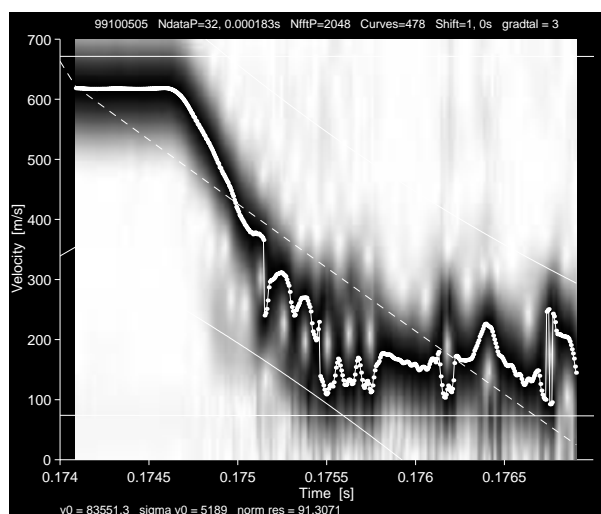
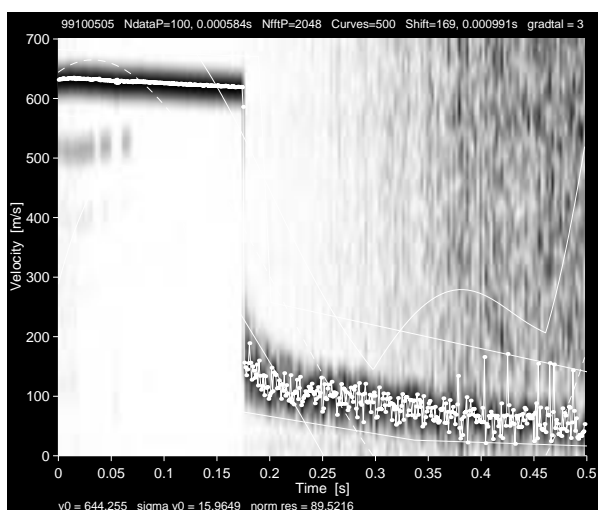


Figure 67. Doppler radar data for target 5

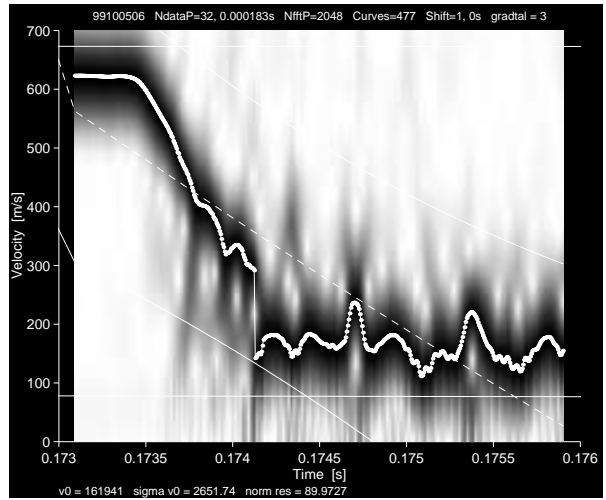
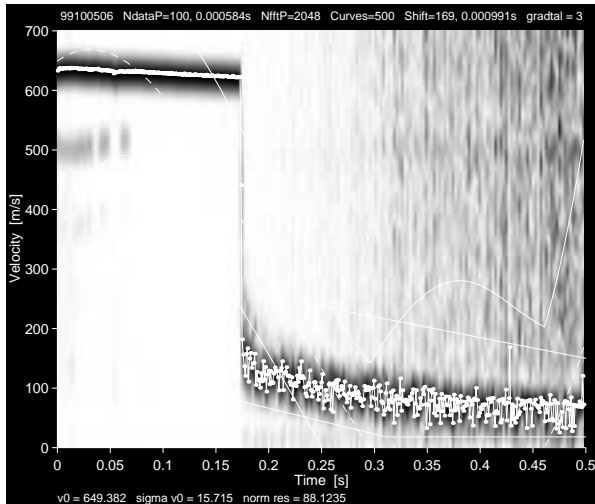


Figure 68. Doppler radar data for target 6

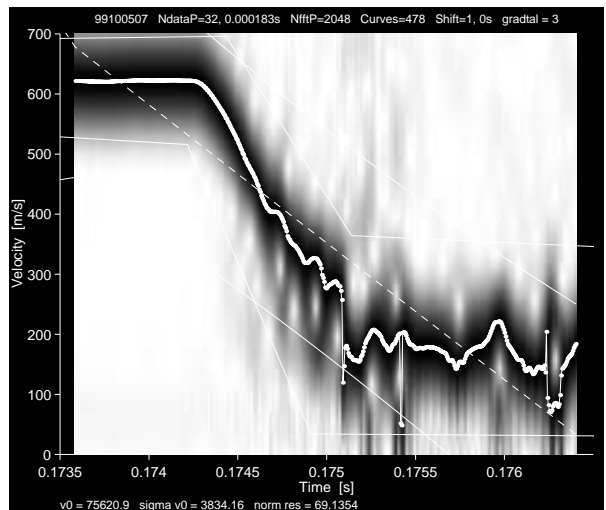
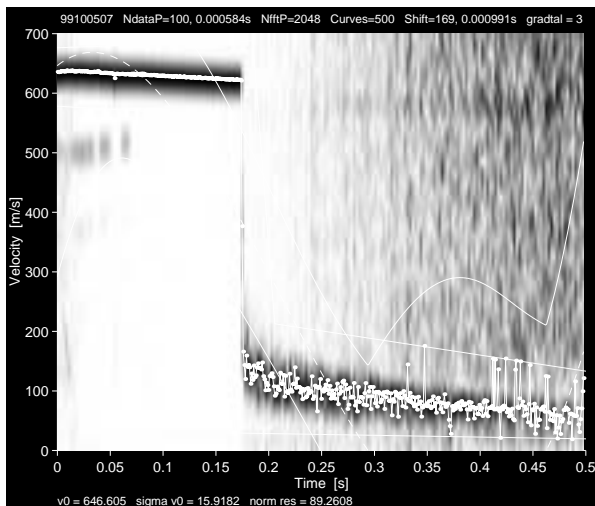


Figure 69. Doppler radar data for target 7

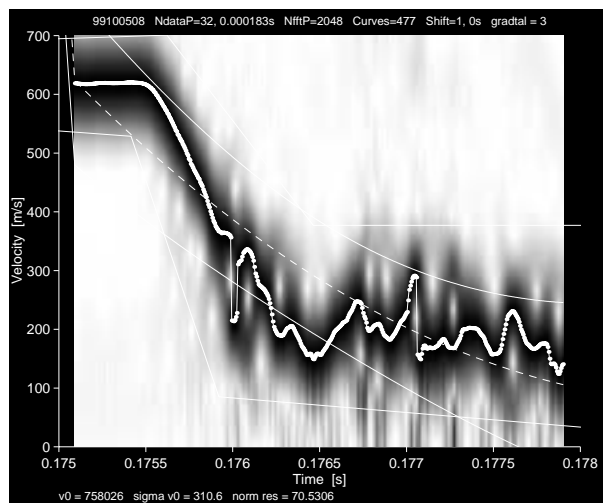
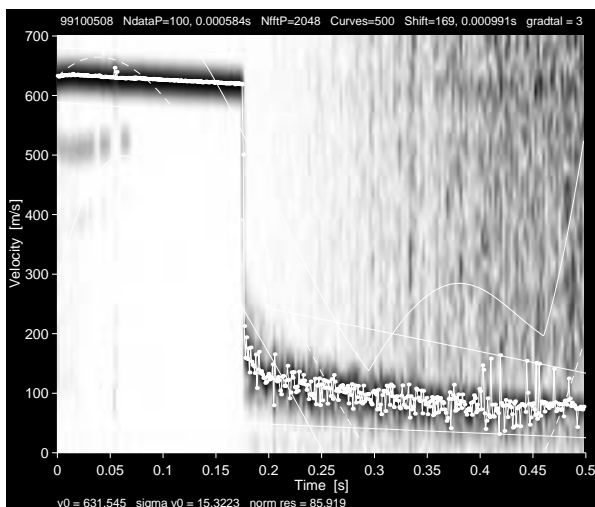


Figure 70. Doppler radar data for target 8

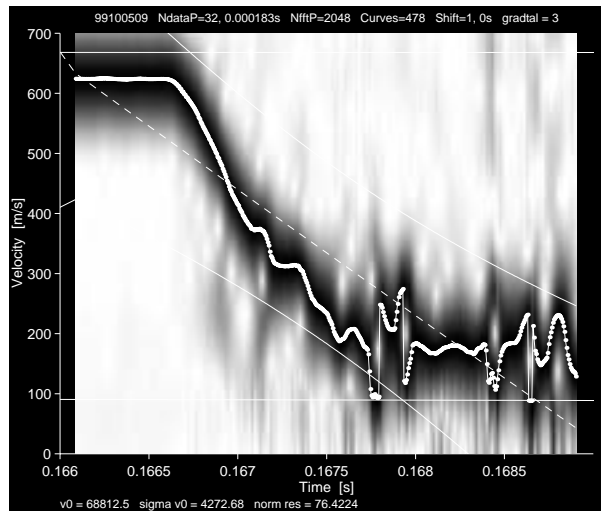
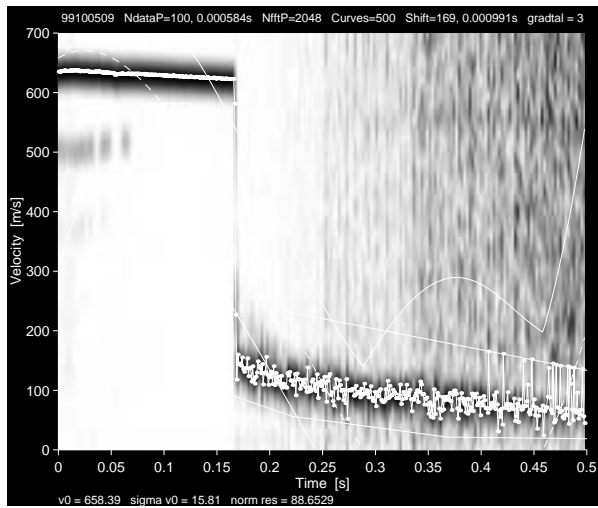


Figure 71. Doppler radar data for target 9

## Appendix B

With the material model "Pseudo Tensor" (LS-DYNA material type 16) as a basis the American company Karagozian & Case released in 1994 a constitutive concrete model for the Defence Nuclear Agency (DNA) Conventional Weapons Effects program. This model is part of the LS-DYNA standard material library since 1996 (version 940) where it is referred to as material type 72 "Concrete Damage". This version of the material model is called release I.

### Strength surfaces

The strength surfaces limits the deviatoric stress at the corresponding pressure and in the model the construction of the strength surface in stress space is based on:

- User input of the uniaxial tensile strength
- User input of a curve for the compression meridian valid for pressures above one third of the uniaxial compression strength, i.e. including the unconfined uniaxial compression test.

$$\Delta\sigma = \sqrt{3J_2} = a_0 + \frac{p}{a_1 + a_2 p}$$

- the assumption that the tri-axial tensile strength is equal to the uniaxial tensile test
- the assumption (based on studies of experimental data) that the bi-axial compressive strength is equal to 1.15 times the uniaxial compressive strength
- the assumption (based on studies of experimental data) that the ratio between the compressive and extension meridian at a pressure of three times the uniaxial compressive strength is 0.753.
- the assumption (based on studies of experimental data) that the ratio between the compressive and extension meridian at pressures higher than 8.45 times the uniaxial compressive strength is 1.
- the 3D-shape proposed by William and Warnke for the strength surface leading to the following expression for the distance from the hydro static pressure axis to an arbitrary point in stress space lying on the strength surface.

$$\frac{r}{r_c} = \frac{2(1-\psi^2)\cos\theta + (2\psi-1)\sqrt{4(1-\psi^2)\cos^2\theta + 5\psi^2 - 4\psi}}{4(1-\psi^2)\cos^2\theta + (1-2\psi)^2}$$

$$\psi(p) = \frac{r_t}{r_c} = \text{relative distance between compression and tension meridian}$$

$$\cos 3\theta = \frac{3\sqrt{3}J_3}{2J_2^{3/2}}$$

- User input of a curve describing the migration between yield, maximum and residual strength surfaces,  $\lambda = \lambda(\eta)$

The compression and extension meridians with stress paths for some tests are schematically shown in Figure B-1 and a schematically strength surface in 3D-stress space is shown in Figure B-2.

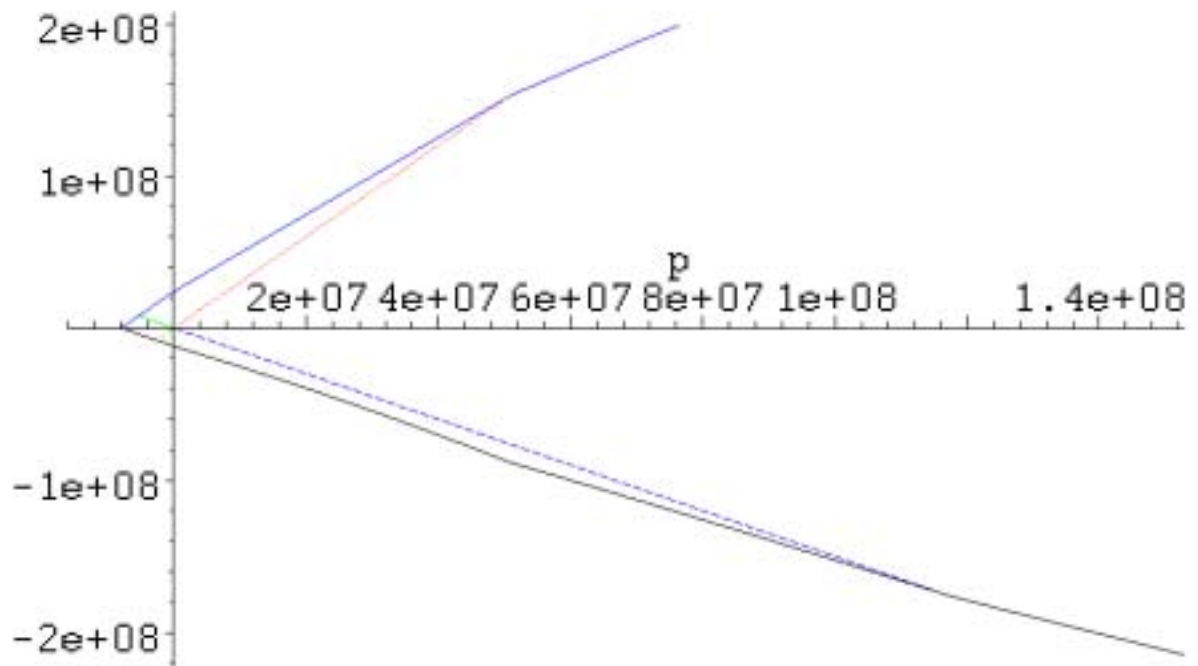


Figure B-1. Compression and extension meridian with stress paths for different tests

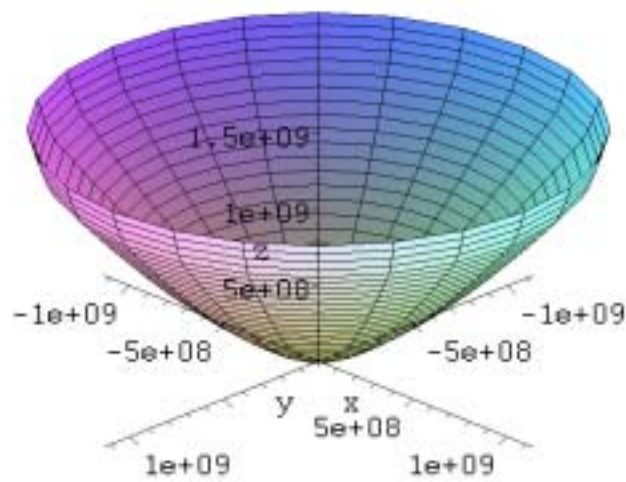


Figure B-2. Strength surface in stress space

### Strength enhancement due to strain rates

The strength enhancement due to strain rates is done along radial stress paths in the stress space. This is in accordance with data from unconfined compressive and tensile tests, but since the enhancement is based on effective strain, the model does not differentiate between compressive and tensile stress paths.

$$\Delta\sigma = r_f \Delta\sigma(p / r_f)$$

$r_f(\epsilon^{effective})$  = Strength enhancement factor

The strength enhancement factor is given by the user as a piecewise linear curve, see Figure B-3 for an example.

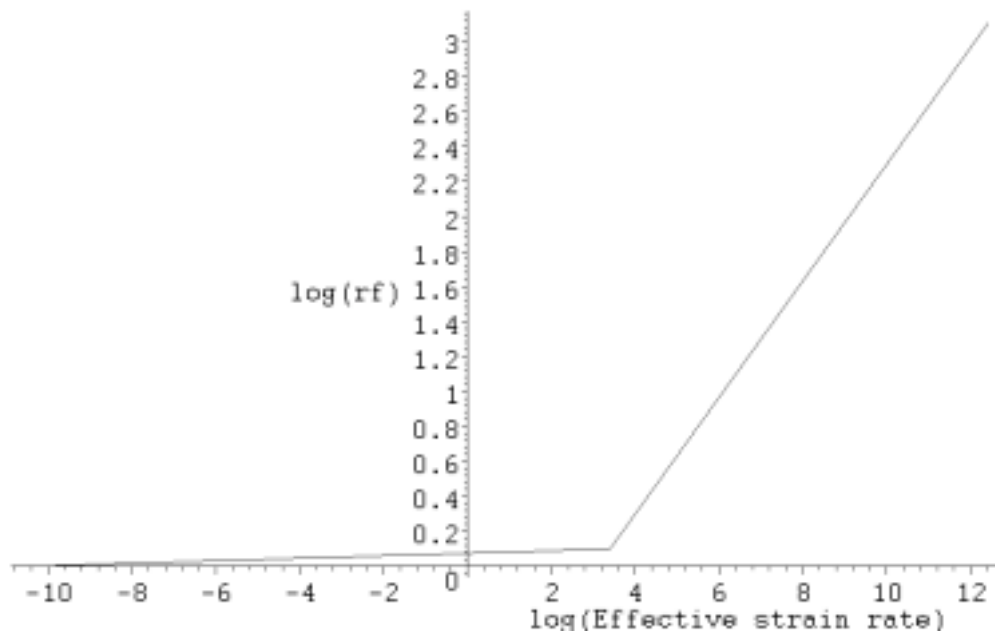
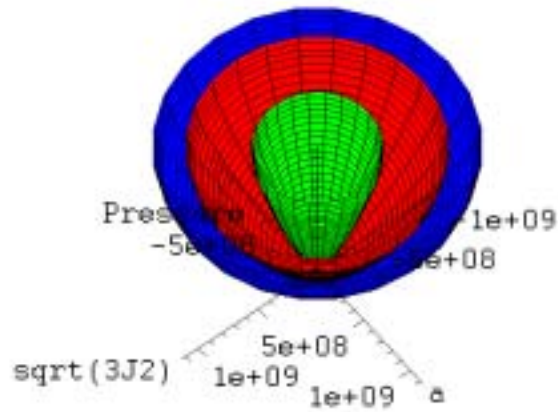


Figure B-3. Example of an strength enhancement function

### Damage accumulation

In order to incorporate yield strength and residual strength two additional surfaces are defined, see Figure B-4 for a schematically representation.



**Figure B-4. Yield (red), max. (blue) and residual (green) strength surfaces in stress space**

During loading the strength surface has to migrate between the three strength surfaces and this is done using the following relations.

$$\Delta\sigma = \eta(\Delta\sigma_{\max} - \Delta\sigma_{\min})\Delta\sigma_{\min}$$

$$p_c = \begin{cases} -f_{ct} \\ -\eta(\lambda)f_{ct} \end{cases}$$

$$\eta = \eta(\lambda)$$

$p_c$  is the pressure cut-off, i.e. the maximum tensile that can be reached,  $\eta$  is the migration function and  $\lambda$  is called the modified effective plastic strain measure and is calculated according to:

$$\lambda = \int_0^{\bar{\epsilon}^p} \frac{d\bar{\epsilon}^p}{r_f \left(1 + \frac{p}{r_f} f_{ct}\right)^{b_i}} + b_3 f_d k_d (\epsilon_v - \epsilon_v^{yield})$$

where

$$d\bar{\varepsilon}^p = \sqrt{\frac{2}{3} \varepsilon_{ij}^p \varepsilon_{ij}^p}$$

$$b_i = \text{scalar multiplier for uniaxial stress states} = \begin{cases} b_1 & \text{for } p \geq 0 \\ b_2 & \text{for } p < 0 \end{cases}$$

$b_3$  = scalar multiplier for triaxial stress states

$$f_d = \begin{cases} 1 - \frac{|p^{-1} \sqrt{3J_2}|}{0.1} & \text{for } 0 \leq |p^{-1} \sqrt{3J_2}| \leq 0.1 \\ 0 & \text{for } |p^{-1} \sqrt{3J_2}| > 0.1 \end{cases}$$

$$k_d = \text{internal scalar multiplier} = -\frac{\varepsilon_v K}{3f_{ct}}$$

$$\varepsilon_v = -\frac{1}{3} \varepsilon_{ii}$$

The function  $\eta(\lambda)$  is given by the user as a piecewise linear curve and the b-parameters are determined through iterative calculations to get the fracture energy right for different stress paths. The parameter  $\eta$  ranges from some start value  $< 1$  representing the yield strength surface, up to 1 for the maximum strength surface and down to 0 for the residual strength surface. An example is given in Figure B-5.

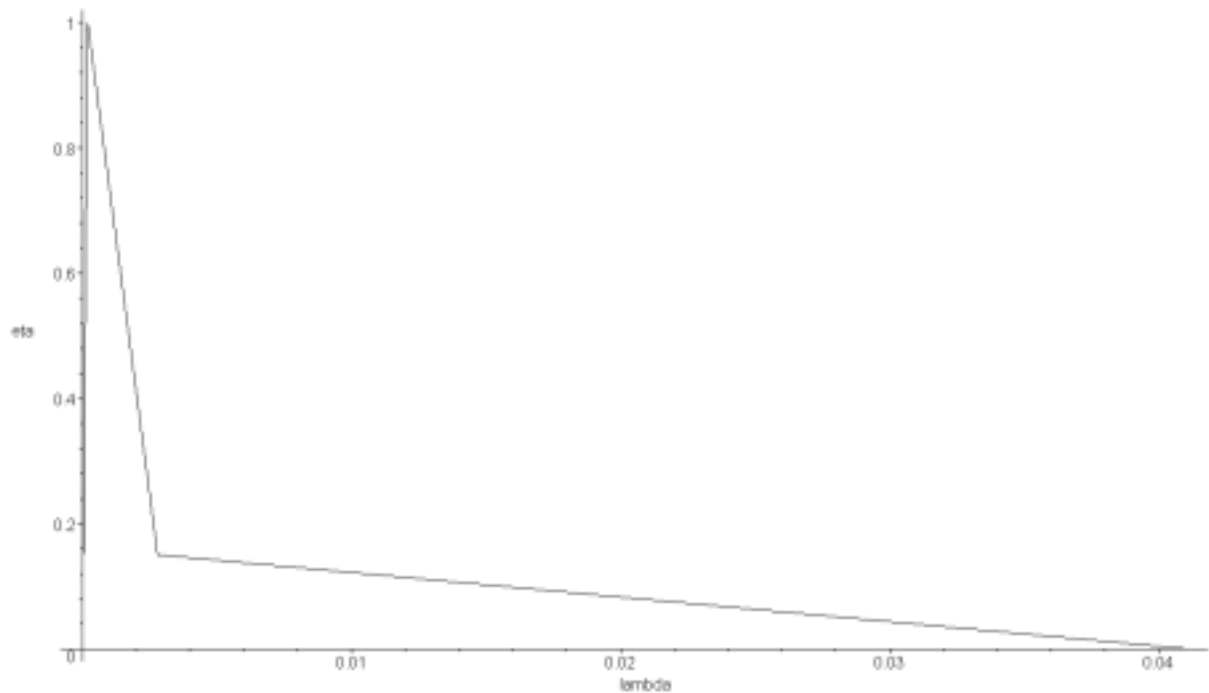


**Figure B-5. Example of a damage function**

In a situation with negative pressure and softening a modified maximum strength surface is used to avoid a vertical pressure cut-off plane in stress space:

$$\Delta\sigma_{\max}^{\text{modified}} = \begin{cases} \eta\Delta\sigma_{\max} + (1-\eta)\Delta\sigma_{\text{res}} & \text{for } p > 0 \\ 3(p + \eta f_{ct}) & \text{for } p \geq 0 \end{cases}$$

Plastic flow

The model uses the volume-preserving Prandtl-Reuss flow rule, i.e. the plastic flow has a radial direction from the hydrostatic pressure axis.

$$f(p, \eta) = \sqrt{3J_2} - Y$$

where  $Y$  is the current position of the strength surface in stress space. The update to the strength surface (after the elastic trial step) becomes

$$Y_{n+1} - Y^* = \frac{Y_n \eta'(\lambda) h(\sigma)}{3G} \frac{f(\sigma^*)}{1 + Y_n \eta'(\lambda) h(\sigma) / 3G}$$

where

$Y^*$  = Updated strength surface due to increment pressure

$$Y_n \begin{cases} r_f [\Delta \sigma_m (p / r_t) - \Delta \sigma_f (p - r_f)], & p \geq p_f, \\ 3r_f f_t, & p < p_f. \end{cases}$$

$$h(\sigma) = r_f \left( 1 + \frac{p}{r_f} f_{ct} \right)^{b_t}$$

The increment for the modified effective plastic strain measure  $\lambda$  is:

$$d\lambda = h(\sigma) d\bar{\varepsilon}^p = h(\sigma) \frac{2}{3} \sqrt{J_2} d\mu = \frac{h(\sigma) [\sqrt{3J_2}^* - Y(p^*, \eta_n)]}{3G \left[ 1 + \frac{Y_n \eta'(\lambda) h(\sigma)}{3G} \right]}$$

### Calculation of shear modulus

The Poisson's ratio is constant and given by the user and the shear modulus is calculated using this value and the bulk modulus from the given equation of state.

$$G = \frac{(1.5 - 3\nu)K'}{1 + \nu}$$

$$K' = (K_L - K_U) e^{-5.55\varphi} + K_U$$

$$\varphi = \frac{-\Delta\varepsilon}{-\Delta\varepsilon + (p - p_f) / K_U}$$

$$\Delta\varepsilon = \varepsilon_{v, \min} - \varepsilon_v$$

where

$K_L$  = Loading bulk modulus

$K_U$  = Unloading bulk modulus

### Release II

A second release of the material model was presented in February 1996, but the model is not implemented in the LS-DYNA material library. The main new capabilities in the model are:

### (1) incorporation of shear dilatancy

Using a flow rule that increments the plastic strain normal to the strength surface, associative flow rule, yields excessive dilatancy (change in volume) in shear. The Prandtl-Reuss flow rule is a special case of a non-associative flow rule that yields no dilatancy at all. From shear tests on concrete it is found that dilatancy occurs, to a certain degree. In release II the introduction of general non-associative flow rule controlled by a input parameter  $\omega$  gives the possibility to handle shear dilatancy.

### (2) different rate enhancement in tension and compression

Tests show that strength enhancement due to strain rate are different in tension than in compression. In release II the possibility is given to account for this via a user defined curve ranging from negative (tensile enhancement) to positive (compressive enhancement) strain rates.

### (3) variable strain enhancement with strain rate

In addition, strain rate dependency on the peak strain has been added which the user controls by entering a scalar representing how large a fraction of the strength enhancement curve to be used for strain enhancement.

## Release III

In release III beta 20 of the material model, the generation of input material parameters has been automated. The parameter generation is based on the concrete compressive strength, the system of units, and the element size (or relative element size). In addition, release III beta 21 is on the way and will be able to handle different element sizes using a unit length conversion factor (a characteristic length).

## Appendix C

Bofors-99, Constitutive model behaviour (SI-units)

```
dn3d kw93
batch

term 1. plti 1.
gmpert elout 1.E-10 nodout 1.E-10;

c ***** PARAMETERS ***
c Load rate
  [lr=1.E-4]

c Element size
  [lch=5.E-3]
c [lch=7.5E-3]

c ***** SYMMETRY PLANES ***
plane 3
  0.  0.  0. -1.  0.  0. 1.E-6 symm
  0.  0.  0.  0. -1.  0. 1.E-6 symm
  0.  0.  0.  0.  0. -1. 1.E-6 symm

c ***** LOAD CURVE ***
c Deformation load curve
lcd 1 2
  0.  1.
  1000. 1.

c ***** MATERIAL DEFINITIONS ***
mat 1
  type 12 brfo 1 hggt 5
  ro 2770 g [50.E+9/(2*(1+.2))] sigy 50.E+6 eh [100.E+6/0.0025] bulk 2.843E+10
endmat

eos 8
  npts 7 gamma 0.0 e0 0.0 v0 1.0
  lnv  0.000000  -0.007034  -0.028960  -0.050979
      -0.062837  -0.072613  -0.144392
  pc    0.      2.E+08    2.4E+08    3.9E+08
      5.65E+08  7.37E+08    2.E+09
  ku   2.843E+10 2.843E+10 2.843E+10 2.843E+10
      2.843E+10 2.843E+10 2.843E+10
endeos

c ***** SPECIMEN PART DEFINITION ***
Start
  1 2;
  1 2;
  1 2;
  0. [.5*lch]
  0. [.5*lch]
  0. [.5*lch]

c Uniaxial compression - b1
  fv 1 1 2 2 2 2 1 [lr] 0. 0. -1. 0. 1000.
  b 1 1 2 2 2 2 000111

c Uniaxial tension - b2
c fv 1 1 2 2 2 2 1 [lr] 0. 0. 1. 0. 1000.
c b 1 1 2 2 2 2 000111

c Triaxial tension - b3
c fv 1 1 2 2 2 2 1 [lr] 0. 0. 1. 0. 1000.
c fv 1 2 1 2 2 2 1 [lr] 0. 1. 0. 0. 1000.
c fv 2 1 1 2 2 2 1 [lr] 1. 0. 0. 0. 1000.
c b 1 1 2 2 2 2 000111
```

```
c b 1 2 1 2 2 2 000111
c b 2 1 1 2 2 2 000111
```

```
npb 1 1 2;
epb 1 1 1;
mat 1
end
```

```
c ***** END ***
end
continue
```

```
c ***** KEYWORD ***
```

```
c 5mm mesh
```

```
*MAT_CONCRETE_DAMAGE
```

```
1 2770 0.16
8.0E+6 50.643E+6 0.465 0.657E-9
22.789E+6 1.033 1.460E-9 0.465 0.657E-9 1.0 1.0 .023
0 0 0 0 0 0 0
0. .02E-3 2.8E-3 41.E-3
0. 1. .15 .0
```

```
c 7.5mm mesh
```

```
*MAT_CONCRETE_DAMAGE
```

```
1 2770 0.16
8.0E+6 50.643E+6 0.465 0.657E-9
22.789E+6 1.033 1.460E-9 0.465 0.657E-9 0.682 6.46 .035
0 0 0 0 0 0 0
0. 1.5E-4 9.E-4 35.E-4
0. 1. .2 .0
```

## Appendix D

Bofors-99, Target 1-3 (SI-units)

dn3d kw93  
batch

term 5.0E-3 plti 1.E-1  
gmprt nodout 1.E-10 elout 1.E-10 matsum 1.E-10;  
taurus int8 8;

c \*\*\*\*\* PARAMETERS \*\*\*  
c Projectile

[v = 616] [r = 0.075 / 2] [nose = 0.090] [length = 0.225]  
[rc = (r\*r+nose\*nose)/2/r] [a = asin(nose/rc)]

c \*\*\*\*\* LOAD CURVES \*\*\*

c Dynamic increase factor (DIF) in compression according to  
c CEB-FIP Model Code 1990

c Linear function.

lcd 1 65

3.00E-05	1.000	3.00E-04	1.017	3.00E-03	1.034	3.00E-02	1.051	3.00E-01	1.069
3.00E+00	1.086	3.00E+01	1.105	4.00E+01	1.107	5.00E+01	1.109	6.00E+01	1.110
7.00E+01	1.111	8.00E+01	1.112	9.00E+01	1.113	1.00E+02	1.114	2.00E+02	1.120
3.00E+02	1.123	4.00E+02	1.125	5.00E+02	1.127	6.00E+02	1.129	7.00E+02	1.130
8.00E+02	1.131	9.00E+02	1.132	1.00E+03	1.133	2.00E+03	1.138	3.00E+03	1.142
4.00E+03	1.144	5.00E+03	1.146	6.00E+03	1.147	7.00E+03	1.149	8.00E+03	1.150
9.00E+03	1.151	1.00E+04	1.152	1.10E+04	1.152	1.20E+04	1.153	1.30E+04	1.154
1.40E+04	1.154	1.50E+04	1.155	1.60E+04	1.156	1.70E+04	1.156	1.80E+04	1.157
1.90E+04	1.157	2.00E+04	1.157	3.00E+04	1.161	4.00E+04	1.163	5.00E+04	1.165
6.00E+04	1.167	7.00E+04	1.168	8.00E+04	1.169	9.00E+04	1.170	1.00E+05	1.171
1.10E+05	1.172	1.20E+05	1.172	1.30E+05	1.173	1.40E+05	1.174	1.50E+05	1.174
1.60E+05	1.175	1.70E+05	1.175	1.80E+05	1.176	1.90E+05	1.176	2.00E+05	1.177
2.10E+05	1.177	2.20E+05	1.178	2.30E+05	1.178	2.40E+05	1.178	2.50E+05	1.179

c Bilinear function.

lcd 2 65

3.00E-05	1.000	3.00E-04	1.017	3.00E-03	1.034	3.00E-02	1.051	3.00E-01	1.069
3.00E+00	1.086	3.00E+01	1.105	4.00E+01	1.216	5.00E+01	1.310	6.00E+01	1.392
7.00E+01	1.465	8.00E+01	1.532	9.00E+01	1.593	1.00E+02	1.650	2.00E+02	2.079
3.00E+02	2.380	4.00E+02	2.619	5.00E+02	2.821	6.00E+02	2.998	7.00E+02	3.156
8.00E+02	3.300	9.00E+02	3.432	1.00E+03	3.555	2.00E+03	4.479	3.00E+03	5.127
4.00E+03	5.643	5.00E+03	6.078	6.00E+03	6.459	7.00E+03	6.800	8.00E+03	7.109
9.00E+03	7.394	1.00E+04	7.658	1.10E+04	7.906	1.20E+04	8.138	1.30E+04	8.358
1.40E+04	8.567	1.50E+04	8.767	1.60E+04	8.957	1.70E+04	9.140	1.80E+04	9.316
1.90E+04	9.485	2.00E+04	9.649	3.00E+04	11.045	4.00E+04	12.157	5.00E+04	13.096
6.00E+04	13.916	7.00E+04	14.650	8.00E+04	15.317	9.00E+04	15.930	1.00E+05	16.499
1.10E+05	17.032	1.20E+05	17.533	1.30E+05	18.007	1.40E+05	18.458	1.50E+05	18.887
1.60E+05	19.298	1.70E+05	19.692	1.80E+05	20.071	1.90E+05	20.436	2.00E+05	20.788
2.10E+05	21.129	2.20E+05	21.459	2.30E+05	21.779	2.40E+05	22.091	2.50E+05	22.393

c \*\*\*\*\* SYMMETRY PLANES \*\*\*

plane 2

0. 0. 0. -1. 0. 0. 1.E-6 symm  
0. 0. 0. 0. -1. 0. 1.E-6 symm

c \*\*\*\*\* INTERFACES \*\*\*

si 1 t14 fd 0.0 material master 1; material slave 2; ;

c \*\*\*\*\* LINES AND SURFACES DEFINITIONS \*\*\*

l3d 1 lp 1 [-r] 0.000 [-nose] lrot [rc-r] 0.000 [-nose] 0 1 0 [-90]  
sd 1 L3S 0 0 0 0 0 1 1  
sd 2 cyli 0 0 0 0 0 1. [r]  
sd 3 cyli 0 0 0 0 0 1. 0.700  
sd 4 cyli 0 0 0 0 0 1. 0.150

c \*\*\*\*\* MATERIAL DEFINITIONS \*\*\*

c Target dummy material

```

mat 1
  type 12
  ro 2770 g [50.E+9/(2*(1+.2))] sigy [0.3*150.E+6] eh [100.E+6/0.0025]
  bulk 17.E+9 hggt 5 brfo 1
endmat

eos 8
  npts 7 gamma 0.0 e0 0.0 v0 1.0
  lnv 0.000000 -0.007034 -0.028960 -0.050979
      -0.062837 -0.072613 -0.144392
  pc      0.      2.E+08      2.4E+08      3.9E+08
      5.65E+08      7.37E+08      2.E+09
  ku 2.843E+10 2.843E+10 2.843E+10 2.843E+10
      2.843E+10 2.843E+10 2.843E+10
endeos

c Projectile
mat 2
  type 1
  ro 7800 e 200.E+9 pr 0.3 hggt 5 brfo 2
endmat

c ***** CONCRETE PART DEFINITION ***
start
c 5mm
c 1 31 58;
c 1 31 58;
c 1 161;

c 7.5mm
  1 21 44;
  1 21 44;
  1 108;

  0.000 0.010 0.010
  0.000 0.010 0.010
  0.000 0.800

  di 2 3; 2 3; 0;

  sfi -3; 1 2; ; sd 3
  sfi 1 2; -3; ; sd 3
  sfvi -2; 1 2; ; sd 4
  sfvi 1 2; -2; ; sd 4

  res 2 1 1 3 2 2 i 1.1
  res 1 2 1 2 3 2 j 1.1

  b 3 1 1 3 2 2 001000
  b 1 3 1 2 3 2 001000

c Elements in impact area
  epb 1 1 1;
  epb 1 1 1 po 0 0 1;
c Element in exiting area
  epb 1 1 2;
c Nodes in impact area to calculate model's maximum strain rates
  npb 1 1 1;
  npb 1 1 1 po 0 0 1;
  npb 1 1 1 po 0 0 2;

  mat 1
end

c ***** PROJECTILE PART DEFINITION ***
start
  1 4 6 8 11;
  1 4 6 8 11;

```

```

1 4 9 19;
[-r/3] [-r/3] 0 [r/3] [r/3]
[-r/3] [-r/3] 0 [r/3] [r/3]
[-nose/3] [-nose/3] [-nose] [-length]

di 1 2 0 4 5; 1 2 0 4 5; ;
di 1 2 0 4 5; ; 1 2;
di ; 1 2 0 4 5; 1 2;
pa 3 3 1 z 0
sfi -1 -5; -1 -5; -1 3; SD 1
sfi -1 -5; -1 -5; 3 4; SD 2
di 1 3; ; ;
di ; 3 5; ;
coord 1 mx -1.E-4 rz [90];
lrep 1;
b 3 1 0 3 3 0 110111
b 3 3 0 5 3 0 110111

c Projectile rear node
npb 3 3 4;
c Nose top element
epb 3 3 1;

mat 2
velocity 0 0 [v]
end

c ***** end ***
end

c ***** LS-INGRID INTERACTIVE COMMANDS ***
tp 1.E-5
cont
stop

c ***** KEYWORD FORMAT ***
*MAT_ADD_EROSION
1
0.9

c 5mm mesh
*MAT_CONCRETE_DAMAGE
1 2770 0.16
8.0E+6 50.643E+6 0.465 0.657E-9
22.789E+6 1.033 1.460E-9 0.465 0.657E-9 1.0 1.0 .023
0 0 0 0 0 0 0
0. .02E-3 2.8E-3 41.E-3
0. 1. .15 .0

c 7.5mm mesh
*MAT_CONCRETE_DAMAGE
1 2770 0.16
8.0E+6 50.643E+6 0.465 0.657E-9
22.789E+6 1.033 1.460E-9 0.465 0.657E-9 0.682 6.46 .035
0 0 0 0 0 0 0
0. 1.5E-4 9.E-4 35.E-4
0. 1. .2 .0

```

## Appendix E

Bofors-99, Target 1-3\_sq (SI-units)

dn3d kw93  
batch

term 5.0E-3 plti 1.E-1  
gmprt nodout 1.E-10 elout 1.E-10 matsum 1.E-10;  
taurus int8 8;

c \*\*\*\*\* PARAMETERS \*\*\*

c Projectile

[v = 616] [r = 0.075 / 2] [nose = 0.090] [length = 0.225]  
[rc = (r\*r+nose\*nose)/2/r] [a = asin(nose/rc)]

c \*\*\*\*\* LOAD CURVES \*\*\*

c Dynamic increase factor (DIF) in compression according to

c CEB-FIP Model Code 1990

c Linear function.

lcd 1 65

3.00E-05	1.000	3.00E-04	1.017	3.00E-03	1.034	3.00E-02	1.051	3.00E-01	1.069
3.00E+00	1.086	3.00E+01	1.105	4.00E+01	1.107	5.00E+01	1.109	6.00E+01	1.110
7.00E+01	1.111	8.00E+01	1.112	9.00E+01	1.113	1.00E+02	1.114	2.00E+02	1.120
3.00E+02	1.123	4.00E+02	1.125	5.00E+02	1.127	6.00E+02	1.129	7.00E+02	1.130
8.00E+02	1.131	9.00E+02	1.132	1.00E+03	1.133	2.00E+03	1.138	3.00E+03	1.142
4.00E+03	1.144	5.00E+03	1.146	6.00E+03	1.147	7.00E+03	1.149	8.00E+03	1.150
9.00E+03	1.151	1.00E+04	1.152	1.10E+04	1.152	1.20E+04	1.153	1.30E+04	1.154
1.40E+04	1.154	1.50E+04	1.155	1.60E+04	1.156	1.70E+04	1.156	1.80E+04	1.157
1.90E+04	1.157	2.00E+04	1.157	3.00E+04	1.161	4.00E+04	1.163	5.00E+04	1.165
6.00E+04	1.167	7.00E+04	1.168	8.00E+04	1.169	9.00E+04	1.170	1.00E+05	1.171
1.10E+05	1.172	1.20E+05	1.172	1.30E+05	1.173	1.40E+05	1.174	1.50E+05	1.174
1.60E+05	1.175	1.70E+05	1.175	1.80E+05	1.176	1.90E+05	1.176	2.00E+05	1.177
2.10E+05	1.177	2.20E+05	1.178	2.30E+05	1.178	2.40E+05	1.178	2.50E+05	1.179

c Bilinear function.

lcd 2 65

3.00E-05	1.000	3.00E-04	1.017	3.00E-03	1.034	3.00E-02	1.051	3.00E-01	1.069
3.00E+00	1.086	3.00E+01	1.105	4.00E+01	1.216	5.00E+01	1.310	6.00E+01	1.392
7.00E+01	1.465	8.00E+01	1.532	9.00E+01	1.593	1.00E+02	1.650	2.00E+02	2.079
3.00E+02	2.380	4.00E+02	2.619	5.00E+02	2.821	6.00E+02	2.998	7.00E+02	3.156
8.00E+02	3.300	9.00E+02	3.432	1.00E+03	3.555	2.00E+03	4.479	3.00E+03	5.127
4.00E+03	5.643	5.00E+03	6.078	6.00E+03	6.459	7.00E+03	6.800	8.00E+03	7.109
9.00E+03	7.394	1.00E+04	7.658	1.10E+04	7.906	1.20E+04	8.138	1.30E+04	8.358
1.40E+04	8.567	1.50E+04	8.767	1.60E+04	8.957	1.70E+04	9.140	1.80E+04	9.316
1.90E+04	9.485	2.00E+04	9.649	3.00E+04	11.045	4.00E+04	12.157	5.00E+04	13.096
6.00E+04	13.916	7.00E+04	14.650	8.00E+04	15.317	9.00E+04	15.930	1.00E+05	16.499
1.10E+05	17.032	1.20E+05	17.533	1.30E+05	18.007	1.40E+05	18.458	1.50E+05	18.887
1.60E+05	19.298	1.70E+05	19.692	1.80E+05	20.071	1.90E+05	20.436	2.00E+05	20.788
2.10E+05	21.129	2.20E+05	21.459	2.30E+05	21.779	2.40E+05	22.091	2.50E+05	22.393

c \*\*\*\*\* SYMMETRY PLANES \*\*\*

plane 2

0. 0. 0. -1. 0. 0. 1.E-6 symm

0. 0. 0. 0. -1. 0. 1.E-6 symm

c \*\*\*\*\* INTERFACES \*\*\*

si 1 t14 fd 0.0 material master 1; material slave 2; ;

c \*\*\*\*\* LINES AND SURFACES DEFINITIONS \*\*\*

l3d 1 lp 1 [-r] 0.000 [-nose] lrot [rc-r] 0.000 [-nose] 0 1 0 [-90]

sd 1 L3S 0 0 0 0 0 1 1

sd 2 cyli 0 0 0 0 0 1. [r]

c \*\*\*\*\* MATERIAL DEFINITIONS \*\*\*

c Target dummy material

mat 1

type 12

```

ro 2770 g [50.E+9/(2*(1+.2))] sigy [0.3*150.E+6] eh [100.E+6/0.0025]
bulk 17.E+9 hgqt 5 brfo 1
endmat

eos 8
npts 7 gamma 0.0 e0 0.0 v0 1.0
lnv 0.000000 -0.007034 -0.028960 -0.050979
    -0.062837 -0.072613 -0.144392
pc 0. 2.E+08 2.4E+08 3.9E+08
    5.65E+08 7.37E+08 2.E+09
ku 2.843E+10 2.843E+10 2.843E+10 2.843E+10
    2.843E+10 2.843E+10 2.843E+10
endeos

c Projectile
mat 2
type 1
ro 7800 e 200.E+9 pr 0.2 hgqt 5 brfo 2
endmat

c ***** CONCRETE PART DEFINITION ***
start
c 5mm square
1 67;
1 67;
1 161;
0 0.330
0 0.330
0 0.800
b 2 1 2 2 2 2 001000
b 1 2 2 2 2 2 001000

c Elements in impact area
epb 1 1 1;
epb 1 1 1 po 0 0 1;
c Element in exiting area
epb 1 1 2;
c Nodes in impact area to calculate model's maximum strain rates
npb 1 1 1;
npb 1 1 1 po 0 0 1;
npb 1 1 1 po 0 0 2;

mat 1
end

c ***** PROJECTILE PART DEFINITION ***
start
1 4 6 8 11;
1 4 6 8 11;
1 4 9 19;
[-r/3] [-r/3] 0 [r/3] [r/3]
[-r/3] [-r/3] 0 [r/3] [r/3]
[-nose/3] [-nose/3] [-nose] [-length]

di 1 2 0 4 5; 1 2 0 4 5; ;
di 1 2 0 4 5; ; 1 2;
di ; 1 2 0 4 5; 1 2;
pa 3 3 1 z 0
sfi -1 -5; -1 -5; -1 3; SD 1
sfi -1 -5; -1 -5; 3 4; SD 2
di 1 3; ; ;
di ; 3 5; ;
coor 1 mx -1.E-4 rz [90];
lrep 1;
b 3 1 0 3 3 0 110111
b 3 3 0 5 3 0 110111

c Projectile rear node

```

```

npb 3 3 4;
c Nose top element
epb 3 3 1;

mat 2
velocity 0 0 [v]
end

c ***** end ***
end

c ***** LS-INGRID INTERACTIVE COMMANDS ***
tp 1.E-5
cont
stop

c ***** KEYWORD FORMAT ***
*MAT_ADD_EROSION
  1
                                0.9

c 5mm mesh
*MAT_CONCRETE_DAMAGE
  1      2770      0.16
  8.0E+6 50.643E+6  0.465  0.657E-9
 22.789E+6  1.033  1.460E-9  0.465  0.657E-9      1.0      1.0      .023
    0      0      0      0      0      0      0
    0.    .02E-3  2.8E-3  41.E-3
    0.      1.      .15      .0

```

## Appendix F

Bofors-99, Target 4-6 (SI-units)

dn3d kw93  
batch

term 2.0E-3 plti 1.E-4  
gmprt nodout 1.E-10 elout 1.E-10 matsum 1.E-10;  
taurus int8 8;

c \*\*\*\*\* PARAMETERS \*\*\*

c Projectile

[v = 617] [r = 0.075 / 2] [nose = 0.090] [length = 0.225]  
[rc = (r\*r+nose\*nose)/2/r] [a = asin(nose/rc)]

c \*\*\*\*\* LOAD CURVES \*\*\*

c Dynamic increase factor (DIF) in compression according to

c CEB-FIP Model Code 1990

c Linear function.

lcd 1 65

3.00E-05	1.000	3.00E-04	1.017	3.00E-03	1.034	3.00E-02	1.051	3.00E-01	1.069
3.00E+00	1.086	3.00E+01	1.105	4.00E+01	1.107	5.00E+01	1.109	6.00E+01	1.110
7.00E+01	1.111	8.00E+01	1.112	9.00E+01	1.113	1.00E+02	1.114	2.00E+02	1.120
3.00E+02	1.123	4.00E+02	1.125	5.00E+02	1.127	6.00E+02	1.129	7.00E+02	1.130
8.00E+02	1.131	9.00E+02	1.132	1.00E+03	1.133	2.00E+03	1.138	3.00E+03	1.142
4.00E+03	1.144	5.00E+03	1.146	6.00E+03	1.147	7.00E+03	1.149	8.00E+03	1.150
9.00E+03	1.151	1.00E+04	1.152	1.10E+04	1.152	1.20E+04	1.153	1.30E+04	1.154
1.40E+04	1.154	1.50E+04	1.155	1.60E+04	1.156	1.70E+04	1.156	1.80E+04	1.157
1.90E+04	1.157	2.00E+04	1.157	3.00E+04	1.161	4.00E+04	1.163	5.00E+04	1.165
6.00E+04	1.167	7.00E+04	1.168	8.00E+04	1.169	9.00E+04	1.170	1.00E+05	1.171
1.10E+05	1.172	1.20E+05	1.172	1.30E+05	1.173	1.40E+05	1.174	1.50E+05	1.174
1.60E+05	1.175	1.70E+05	1.175	1.80E+05	1.176	1.90E+05	1.176	2.00E+05	1.177
2.10E+05	1.177	2.20E+05	1.178	2.30E+05	1.178	2.40E+05	1.178	2.50E+05	1.179

c Bilinear function.

lcd 2 65

3.00E-05	1.000	3.00E-04	1.017	3.00E-03	1.034	3.00E-02	1.051	3.00E-01	1.069
3.00E+00	1.086	3.00E+01	1.105	4.00E+01	1.216	5.00E+01	1.310	6.00E+01	1.392
7.00E+01	1.465	8.00E+01	1.532	9.00E+01	1.593	1.00E+02	1.650	2.00E+02	2.079
3.00E+02	2.380	4.00E+02	2.619	5.00E+02	2.821	6.00E+02	2.998	7.00E+02	3.156
8.00E+02	3.300	9.00E+02	3.432	1.00E+03	3.555	2.00E+03	4.479	3.00E+03	5.127
4.00E+03	5.643	5.00E+03	6.078	6.00E+03	6.459	7.00E+03	6.800	8.00E+03	7.109
9.00E+03	7.394	1.00E+04	7.658	1.10E+04	7.906	1.20E+04	8.138	1.30E+04	8.358
1.40E+04	8.567	1.50E+04	8.767	1.60E+04	8.957	1.70E+04	9.140	1.80E+04	9.316
1.90E+04	9.485	2.00E+04	9.649	3.00E+04	11.045	4.00E+04	12.157	5.00E+04	13.096
6.00E+04	13.916	7.00E+04	14.650	8.00E+04	15.317	9.00E+04	15.930	1.00E+05	16.499
1.10E+05	17.032	1.20E+05	17.533	1.30E+05	18.007	1.40E+05	18.458	1.50E+05	18.887
1.60E+05	19.298	1.70E+05	19.692	1.80E+05	20.071	1.90E+05	20.436	2.00E+05	20.788
2.10E+05	21.129	2.20E+05	21.459	2.30E+05	21.779	2.40E+05	22.091	2.50E+05	22.393

c \*\*\*\*\* SYMMETRY PLANES \*\*\*

plane 2

0. 0. 0. -1. 0. 0. 1.E-6 symm  
0. 0. 0. 0. -1. 0. 1.E-6 symm

c \*\*\*\*\* INTERFACES \*\*\*

si 1 t14 fd 0.0 material master 1; material slave 2; ;

c \*\*\*\*\* LINES AND SURFACES DEFINITIONS \*\*\*

l3d 1 lp 1 [-r] 0.000 [-nose] lrot [rc-r] 0.000 [-nose] 0 1 0 [-90]  
sd 1 L3S 0 0 0 0 0 1 1  
sd 2 cyli 0 0 0 0 0 1. [r]  
sd 3 cyli 0 0 0 0 0 1. 0.700  
sd 4 cyli 0 0 0 0 0 1. 0.150

c \*\*\*\*\* MATERIAL DEFINITIONS \*\*\*

c Dummy material - replace in LS-DYNA keyword file with card at end.

```

mat 1
  type 12
  ro 2770 g [50.E+9/(2*(1+.2))] sigy [0.3*150.E+6] eh [100.E+6/0.0025]
  bulk 17.E+9 hqgt 5 brfo 1
endmat

```

```

eos 8
  npts 7 gamma 0.0 e0 0.0 v0 1.0
  lnv 0.000000 -0.007034 -0.028960 -0.050979
      -0.062837 -0.072613 -0.144392
  pc 0. 2.E+08 2.4E+08 3.9E+08
      5.65E+08 7.37E+08 2.E+09
  ku 2.843E+10 2.843E+10 2.843E+10 2.843E+10
      2.843E+10 2.843E+10 2.843E+10
endeos

```

```

mat 2
  type 1
  ro 7800 e 200.E+9 pr 0.3 brfo 2
endmat

```

c \*\*\*\*\* CONCRETE PART DEFINITION \*\*\*

```

start
c 5mm
  1 31 58;
  1 31 58;
  1 81;

c 7.5mm
c 1 21 44;
c 1 21 44;
c 1 54;

0.000 0.010 0.010
0.000 0.010 0.010
0.000 0.400

di 2 3; 2 3; 0;

sfi -3; 1 2; ; sd 3
sfi 1 2; -3; ; sd 3
sfvi -2; 1 2; ; sd 4
sfvi 1 2; -2; ; sd 4

res 2 1 1 3 2 2 i 1.1
res 1 2 1 2 3 2 j 1.1

b 3 1 1 3 2 2 001000
b 1 3 1 2 3 2 001000

c Elements in impact area
  epb 1 1 1;
  epb 1 1 1 po 0 0 1;
c Element in exiting area
  epb 1 1 2;
c Nodes in impact area to calculate model's maximum strain rates
  npb 1 1 1;
  npb 1 1 1 po 0 0 1;
  npb 1 1 1 po 0 0 2;

mat 1
end

```

c \*\*\*\*\* PROJECTILE PART DEFINITION \*\*\*

```

start
  1 4 6 8 11;
  1 4 6 8 11;
  1 4 9 19;

```

```

[-r/3] [-r/3] 0 [r/3] [r/3]
[-r/3] [-r/3] 0 [r/3] [r/3]
[-nose/3] [-nose/3] [-nose] [-length]

di 1 2 0 4 5; 1 2 0 4 5; ;
di 1 2 0 4 5; ; 1 2;
di ; 1 2 0 4 5; 1 2;
pa 3 3 1 z 0
sfi -1 -5; -1 -5; -1 3; SD 1
sfi -1 -5; -1 -5; 3 4; SD 2
di 1 3; ; ;
di ; 3 5; ;
coor 1 mx -1.E-4 rz [90];
lrep 1;
b 3 1 0 3 3 0 110111
b 3 3 0 5 3 0 110111

c Projectile rear node
npb 3 3 4;
c Nose top element
epb 3 3 1;

mat 2
velocity 0 0 [v]
end

c ***** end ***
end

c ***** LS-INGRID INTERACTIVE COMMANDS ***
tp 1.E-5
cont
stop

c ***** KEYWORD FORMAT ***
*MAT_ADD_EROSION
1
0.8

c 5mm mesh
*MAT_CONCRETE_DAMAGE
1 2770 0.16
8.0E+6 50.643E+6 0.465 0.657E-9
22.789E+6 1.033 1.460E-9 0.465 0.657E-9 1.0 1.0 .023
0 0 0 0 0 0 0
0. .02E-3 2.8E-3 41.E-3
0. 1. .15 .0

c 7.5mm mesh
*MAT_CONCRETE_DAMAGE
1 2770 0.16
8.0E+6 50.643E+6 0.465 0.657E-9
22.789E+6 1.033 1.460E-9 0.465 0.657E-9 0.682 6.46 .035
0 0 0 0 0 0 0
0. 1.5E-4 9.E-4 35.E-4
0. 1. .2 .0

```

## Appendix G

Bofors-99, Target 7-9 (SI-units)

dn3d kw93  
batch

term 2.0E-3 plti 1.E-4  
gmprt nodout 1.E-10 elout 1.E-10 matsum 1.E-10;  
taurus int8 8;

c \*\*\*\*\* PARAMETERS \*\*\*

c Projectile

[v = 616] [r = 0.075 / 2] [nose = 0.090] [length = 0.225]  
[rc = (r\*r+nose\*nose)/2/r] [a = asin(nose/rc)]

c \*\*\*\*\* LOAD CURVES \*\*\*

c Dynamic increase factor (DIF) in compression according to

c CEB-FIP Model Code 1990

c Linear function.

lcd 1 65

3.00E-05	1.000	3.00E-04	1.017	3.00E-03	1.034	3.00E-02	1.051	3.00E-01	1.069
3.00E+00	1.086	3.00E+01	1.105	4.00E+01	1.107	5.00E+01	1.109	6.00E+01	1.110
7.00E+01	1.111	8.00E+01	1.112	9.00E+01	1.113	1.00E+02	1.114	2.00E+02	1.120
3.00E+02	1.123	4.00E+02	1.125	5.00E+02	1.127	6.00E+02	1.129	7.00E+02	1.130
8.00E+02	1.131	9.00E+02	1.132	1.00E+03	1.133	2.00E+03	1.138	3.00E+03	1.142
4.00E+03	1.144	5.00E+03	1.146	6.00E+03	1.147	7.00E+03	1.149	8.00E+03	1.150
9.00E+03	1.151	1.00E+04	1.152	1.10E+04	1.152	1.20E+04	1.153	1.30E+04	1.154
1.40E+04	1.154	1.50E+04	1.155	1.60E+04	1.156	1.70E+04	1.156	1.80E+04	1.157
1.90E+04	1.157	2.00E+04	1.157	3.00E+04	1.161	4.00E+04	1.163	5.00E+04	1.165
6.00E+04	1.167	7.00E+04	1.168	8.00E+04	1.169	9.00E+04	1.170	1.00E+05	1.171
1.10E+05	1.172	1.20E+05	1.172	1.30E+05	1.173	1.40E+05	1.174	1.50E+05	1.174
1.60E+05	1.175	1.70E+05	1.175	1.80E+05	1.176	1.90E+05	1.176	2.00E+05	1.177
2.10E+05	1.177	2.20E+05	1.178	2.30E+05	1.178	2.40E+05	1.178	2.50E+05	1.179

c Bilinear function.

lcd 2 65

3.00E-05	1.000	3.00E-04	1.017	3.00E-03	1.034	3.00E-02	1.051	3.00E-01	1.069
3.00E+00	1.086	3.00E+01	1.105	4.00E+01	1.216	5.00E+01	1.310	6.00E+01	1.392
7.00E+01	1.465	8.00E+01	1.532	9.00E+01	1.593	1.00E+02	1.650	2.00E+02	2.079
3.00E+02	2.380	4.00E+02	2.619	5.00E+02	2.821	6.00E+02	2.998	7.00E+02	3.156
8.00E+02	3.300	9.00E+02	3.432	1.00E+03	3.555	2.00E+03	4.479	3.00E+03	5.127
4.00E+03	5.643	5.00E+03	6.078	6.00E+03	6.459	7.00E+03	6.800	8.00E+03	7.109
9.00E+03	7.394	1.00E+04	7.658	1.10E+04	7.906	1.20E+04	8.138	1.30E+04	8.358
1.40E+04	8.567	1.50E+04	8.767	1.60E+04	8.957	1.70E+04	9.140	1.80E+04	9.316
1.90E+04	9.485	2.00E+04	9.649	3.00E+04	11.045	4.00E+04	12.157	5.00E+04	13.096
6.00E+04	13.916	7.00E+04	14.650	8.00E+04	15.317	9.00E+04	15.930	1.00E+05	16.499
1.10E+05	17.032	1.20E+05	17.533	1.30E+05	18.007	1.40E+05	18.458	1.50E+05	18.887
1.60E+05	19.298	1.70E+05	19.692	1.80E+05	20.071	1.90E+05	20.436	2.00E+05	20.788
2.10E+05	21.129	2.20E+05	21.459	2.30E+05	21.779	2.40E+05	22.091	2.50E+05	22.393

c \*\*\*\*\* SYMMETRY PLANES \*\*\*

plane 2

0. 0. 0. -1. 0. 0. 1.E-6 symm  
0. 0. 0. 0. -1. 0. 1.E-6 symm

c \*\*\*\*\* INTERFACES \*\*\*

si 1 t14 fd 0.0 material master 1; material slave 2; ;

c \*\*\*\*\* LINES AND SURFACES DEFINITIONS \*\*\*

l3d 1 lp 1 [-r] 0.000 [-nose] lrot [rc-r] 0.000 [-nose] 0 1 0 [-90]  
sd 1 L3S 0 0 0 0 0 1 1  
sd 2 cyli 0 0 0 0 0 1. [r]

c \*\*\*\*\* MATERIAL DEFINITIONS \*\*\*

c Target dummy material

mat 1  
type 12

```

ro 2770 g [50.E+9/(2*(1+.2))] sigy [0.3*150.E+6] eh [100.E+6/0.0025]
bulk 17.E+9 hgqt 5 brfo 1
endmat

eos 8
npts 7 gamma 0.0 e0 0.0 v0 1.0
lnv 0.000000 -0.007034 -0.028960 -0.050979
    -0.062837 -0.072613 -0.144392
pc 0. 2.E+08 2.4E+08 3.9E+08
    5.65E+08 7.37E+08 2.E+09
ku 2.843E+10 2.843E+10 2.843E+10 2.843E+10
    2.843E+10 2.843E+10 2.843E+10
endeos

c Projectile
mat 2
type 1
ro 7800 e 200.E+9 pr 0.2 hgqt 5 brfo 2
endmat

c Rebars
mat 3
type 3
ro 7800 e 207.E+9 pr 0.3 sigy 586.E+6 etan 623.E+6 beta 0.5 fs 0.16
beam bform truss care 491.E-6
endmat

c Stirrups
mat 4
type 3
ro 7800 e 207.E+9 pr 0.3 sigy 586.E+6 etan 623.E+6 beta 0.5 fs 0.16
beam bform truss care 113.E-6
endmat

c ***** CONCRETE PART DEFINITION *****
start
c 5mm
1 13 37 49 57 63 67 69;
1 13 37 49 57 63 67 69;
1 9 14 39 44 69 74 81;

0. 0.060 0.180 0.300 0.420 0.540 0.660 0.700
0. 0.060 0.180 0.300 0.420 0.540 0.660 0.700
0. 0.0375 0.0625 0.1875 0.2125 0.3375 0.3625 0.400

b 8 1 1 8 8 8 001000
b 1 8 1 8 8 8 001000

c Elements in impact area
epb 1 1 1;
epb 1 1 1 po 0 0 1;
c Element in exiting area
epb 1 1 8;
c Nodes in impact area to calculate model's maximum strain rates
npb 1 1 1;
npb 1 1 1 po 0 0 1;
npb 1 1 1 po 0 0 2;

mat 1
end

c ***** PROJECTILE PART DEFINITION *****
start
1 4 6 8 11;
1 4 6 8 11;
1 4 9 19;
[-r/3] [-r/3] 0 [r/3] [r/3]
[-r/3] [-r/3] 0 [r/3] [r/3]

```

```

[-nose/3] [-nose/3] [-nose] [-length]

di 1 2 0 4 5; 1 2 0 4 5; ;
di 1 2 0 4 5; ; 1 2;
di ; 1 2 0 4 5; 1 2;
pa 3 3 1 z 0
sfi -1 -5; -1 -5; -1 3; SD 1
sfi -1 -5; -1 -5; 3 4; SD 2
di 1 3; ; ;
di ; 3 5; ;
coord 1 mx -1.E-4 rz [90];
lrep 1;
b 3 1 0 3 3 0 110111
b 3 3 0 5 3 0 110111

c Projectile rear node
npb 3 3 4;
c Nose top element
epb 3 3 1;

mat 2
velocity 0 0 [v]
end

c ***** REINFORCEMENT DEFINITION *****
beam
rt 000000 0.000 0.000 0.000
rt 000000 0.060 0.000 0.000
rt 000000 0.180 0.000 0.000
rt 000000 0.300 0.000 0.000
rt 000000 0.420 0.000 0.000
rt 000000 0.540 0.000 0.000
rt 000000 0.660 0.000 0.000

rt 111111 0.000 0.000 1.000
0
c 5mm
1 2 12 3 1 8
2 3 24 3 1 8
3 4 24 3 1 8
4 5 24 3 1 8
5 6 24 3 1 8
6 7 24 3 1 8
0
coord 36
my 0.060 mz 0.0375;
my 0.180 mz 0.0375;
my 0.300 mz 0.0375;
my 0.420 mz 0.0375;
my 0.540 mz 0.0375;
my 0.660 mz 0.0375;

my -0.060 mz 0.0625 rz 90;
my -0.180 mz 0.0625 rz 90;
my -0.300 mz 0.0625 rz 90;
my -0.420 mz 0.0625 rz 90;
my -0.540 mz 0.0625 rz 90;
my -0.660 mz 0.0625 rz 90;

my 0.060 mz 0.1875;
my 0.180 mz 0.1875;
my 0.300 mz 0.1875;
my 0.420 mz 0.1875;
my 0.540 mz 0.1875;
my 0.660 mz 0.1875;

my -0.060 mz 0.2125 rz 90;
my -0.180 mz 0.2125 rz 90;

```

```
my -0.300 mz 0.2125 rz 90;  
my -0.420 mz 0.2125 rz 90;  
my -0.540 mz 0.2125 rz 90;  
my -0.660 mz 0.2125 rz 90;
```

```
my -0.060 mz 0.3375 rz 90;  
my -0.180 mz 0.3375 rz 90;  
my -0.300 mz 0.3375 rz 90;  
my -0.420 mz 0.3375 rz 90;  
my -0.540 mz 0.3375 rz 90;  
my -0.660 mz 0.3375 rz 90;
```

```
my 0.060 mz 0.3625;  
my 0.180 mz 0.3625;  
my 0.300 mz 0.3625;  
my 0.420 mz 0.3625;  
my 0.540 mz 0.3625;  
my 0.660 mz 0.3625;
```

```
lrep 1 2 3 4 5 6 7 8 9 10 11 12 13 14 15 16 17 18 19 20 21 22 23 24 25 26 27  
28 29 30 31 32 33 34 35 36
```

end

c \*\*\*\*\* STIRRUPS DEFINITION \*\*\*\*\*

beam

```
rt 000000 0.000 0.000 0.0375  
rt 000000 0.000 0.000 0.0625  
rt 000000 0.000 0.000 0.1875  
rt 000000 0.000 0.000 0.2125  
rt 000000 0.000 0.000 0.3375  
rt 000000 0.000 0.000 0.3625  
rt 111111 1.000 0.000 0.000
```

0

```
1 2 5 4 1 7  
2 3 25 4 1 7  
3 4 5 4 1 7  
4 5 25 4 1 7  
5 6 5 4 1 7
```

0

coor 36

```
mx 0.060 my 0.060;  
mx 0.060 my 0.180;  
mx 0.060 my 0.300;  
mx 0.060 my 0.420;  
mx 0.060 my 0.540;  
mx 0.060 my 0.660;
```

```
mx 0.180 my 0.060;  
mx 0.180 my 0.180;  
mx 0.180 my 0.300;  
mx 0.180 my 0.420;  
mx 0.180 my 0.540;  
mx 0.180 my 0.660;
```

```
mx 0.300 my 0.060;  
mx 0.300 my 0.180;  
mx 0.300 my 0.300;  
mx 0.300 my 0.420;  
mx 0.300 my 0.540;  
mx 0.300 my 0.660;
```

```
mx 0.420 my 0.060;  
mx 0.420 my 0.180;  
mx 0.420 my 0.300;  
mx 0.420 my 0.420;  
mx 0.420 my 0.540;  
mx 0.420 my 0.660;
```

```

mx 0.540 my 0.060;
mx 0.540 my 0.180;
mx 0.540 my 0.300;
mx 0.540 my 0.420;
mx 0.540 my 0.540;
mx 0.540 my 0.660;

mx 0.660 my 0.060;
mx 0.660 my 0.180;
mx 0.660 my 0.300;
mx 0.660 my 0.420;
mx 0.660 my 0.540;
mx 0.660 my 0.660;

lrep 1 2 3 4 5 6 7 8 9 10 11 12 13 14 15 16 17 18 19 20 21 22 23 24 25 26 27
     28 29 30 31 32 33 34 35 36
end

c ***** end ***
end

c ***** LS-INGRID INTERACTIVE COMMANDS ***
tp 1.E-5
cont
stop

c ***** KEYWORD FORMAT ***
*MAT_ADD_EROSION
  1
                                0.9

c 5mm mesh
*MAT_CONCRETE_DAMAGE
  1      2770      0.16
  8.0E+6 50.643E+6  0.465 0.657E-9
 22.789E+6  1.033 1.460E-9  0.465 0.657E-9  1.0  1.0  .023
  0      0      0      0      0      0      0
  0.    .02E-3  2.8E-3  41.E-3
  0.      1.      .15      .0

c 7.5mm mesh
*MAT_CONCRETE_DAMAGE
  1      2770      0.16
  8.0E+6 50.643E+6  0.465 0.657E-9
 22.789E+6  1.033 1.460E-9  0.465 0.657E-9  0.682  6.46  .035
  0      0      0      0      0      0      0
  0.    1.5E-4  9.E-4  35.E-4
  0.      1.      .2      .0

```